Supplementary Materials:

New palladium(II) β-ketoesterates for Focused Electron Beam Induced Deposition: Synthesis, structures, and characterization

A. Butrymowicz-Kubiak[1], T.M. Muzioł[1], A. Kaczmarek-Kędziera[1], C. S. Jureddy[2], K. Maćkosz[2], I. Utke[2], I. B. Szymańska[1]*

[1]Faculty of Chemistry, Nicolaus Copernicus University in Toruń, Gagarina 7, 87-100 Toruń, Poland

[2]Empa - Swiss Federal Laboratories for Materials Science and Technology, Laboratory for Mechanics of Materials and Nanostructures, Feuerwerkerstrasse 39, CH - 3602 Thun, Switzerland

X-ray crystal structure determination

Table S 1 Crystal data and structure refinement for (**1−3**).

Identification code	**(1)**	**(2)**	**(3)**
Empirical formula	C16 H26 O6 Pd	C14 H22 O6 Pd	C12 H18 O6 Pd
Formula weight	420.77	392.71	364.66
Temperature [K]	100(2) K	100(2) K	100.15 K
Wavelength [Å]	1.54184 Å	1.54184 Å	1.54184 Å
Crystal system, space group	Triclinic, P-1	Monoclinic, $P2_1/n$	Triclinic, P-1
Unit cell dimensions [Å] and [°]	a = 10.23141(11) Å α = 91.9303(9)° b = 12.95320(14) Å β = 98.1743(9)° c = 14.56071(17) Å γ = 100.3549(9)°	a = 4.35329(10) Å α = 90° b = 10.3794(3) Å β = 93.392(2)° c = 17.7657(5) Å γ = 90°	a = 7.0247(2) Å α = 89.994(3)° b = 8.6043(3) Å β = 80.180(3)° c = 11.5706(4) Å γ = 79.606(3)°
Volume [Å³]	1875.53(4) $Å^3$	801.33(4) $Å^3$	677.46(4) $Å^3$
Z, Calculated density [Mg×m⁻³]	4, 1.490 Mg/m^3	2, 1.628 Mg/m^3	2, 1.788 Mg/m^3
Absorption coefficient [mm⁻¹]	8.207 mm^{-1}	9.558 mm^{-1}	11.252 mm^{-1}
F(000)	864	400	368
Crystal size [mm]	0.140 x 0.060 x 0.030 mm^3	0.130 x 0.040 x 0.020 mm^3	0.1 x 0.03 x 0.02 mm^3
Theta range for data collection [°]	3.072 to 74.503°	4.937 to 74.504°	3.879 to 74.475°
Limiting indices	-12<=h<=12 -16<=k<=16 -16<=l<=18	-5<=h<=4 -12<=k<=12 -17<=l<=22	-8<=h<=8 -10<=k<=7 -14<=l<=14
Reflections collected/unique	68027	5007	8513
Completeness [%] to theta [°]	99.9 %	98.6 %	99.9 %
Absorption correction	Gaussian	Gaussian	Gaussian
Max. and min. transmission	0.908 and 0.490	0.942 and 0.422	0.920 and 0.433
Refinement method	Full-matrix least-squares on F^2	Full-matrix least-squares on F^2	Full-matrix least-squares on F^2
Data/restraints/parameters	7650 / 0 / 432	1605 / 0 / 100	2756 / 0 / 179
Goodness-of-fit on F²	1.052	1.112	1.092
Final R Indices [I>2sigma(I)]	R1 = 0.0184, wR2 = 0.0500	R1 = 0.0346, wR2 = 0.0948	R1 = 0.0261, wR2 = 0.0746
R indices (all data)	R1 = 0.0189, wR2 = 0.0503	R1 = 0.0384, wR2 = 0.0981	R1 = 0.0286, wR2 = 0.0765
Largest diff. peak and hole [eÅ⁻³]	0.372 and -0.545 e. $Å^{-3}$	0.980 and -0.906 e. $Å^{-3}$	0.919 and -0.990 e. $Å^{-3}$

Table S 2 Bond lengths [Å] and angles [°] for [Pd(tbaoac)$_2$] (**1**).

Pd(1)-O(12)	1.9657(11)
Pd(1)-O(2)	1.9710(11)
Pd(1)-O(6)	1.9947(11)
Pd(1)-O(16)	1.9978(11)
Pd(2)-O(22)	1.9628(11)
Pd(2)-O(32)	1.9660(11)
Pd(2)-O(36)	1.9972(11)
Pd(2)-O(26)	2.0010(11)
O(12)-Pd(1)-O(2)	85.30(5)
O(12)-Pd(1)-O(6)	179.55(5)
O(2)-Pd(1)-O(6)	94.70(4)
O(12)-Pd(1)-O(16)	94.88(4)
O(2)-Pd(1)-O(16)	179.71(5)
O(6)-Pd(1)-O(16)	85.11(4)
C(2)-O(2)-Pd(1)	122.69(10)
C(4)-O(6)-Pd(1)	122.82(10)
C(12)-O(12)-Pd(1)	122.83(10)
C(14)-O(16)-Pd(1)	122.59(10)
O(22)-Pd(2)-O(32)	84.38(5)
O(22)-Pd(2)-O(36)	178.04(5)
O(32)-Pd(2)-O(36)	94.34(5)
O(22)-Pd(2)-O(26)	94.95(5)
O(32)-Pd(2)-O(26)	175.70(5)
O(36)-Pd(2)-O(26)	86.44(5)
C(22)-O(22)-Pd(2)	122.88(10)
C(24)-O(26)-Pd(2)	121.38(10)
C(32)-O(32)-Pd(2)	123.17(10)
C(34)-O(36)-Pd(2)	122.89(10)

Symmetry transformations used to generate equivalent atoms:
#1 -x,-y+1,-z+1

Table S 3 Bond lengths [Å] and angles [°] for [Pd(ipaoac)$_2$] (**2**).

Pd(1)-O(1)#1	1.9811(19)
Pd(1)-O(1)	1.9811(19)
Pd(1)-O(4)	1.999(3)
Pd(1)-O(4)#1	1.999(3)
O(1)#1-Pd(1)-O(1)	180.00(9)
O(1)#1-Pd(1)-O(4)	85.23(8)
O(1)-Pd(1)-O(4)	94.77(8)
O(1)#1-Pd(1)-O(4)#1	94.78(8)
O(1)-Pd(1)-O(4)#1	85.22(8)
O(4)-Pd(1)-O(4)#1	180.0
C(2)-O(1)-Pd(1)	122.62(18)
C(4)-O(4)-Pd(1)	122.20(19)

Symmetry transformations used to generate equivalent atoms:
#1 -x,-y+1,-z+1

Table S 4 Bond lengths [Å] and angles [°] for [Pd(eaoac)$_2$] (**3**).

Pd(1)-O(3A)#1	1.9923(15)
Pd(1)-O(3A)	1.9923(15)
Pd(1)-O(5)#1	1.9833(15)
Pd(1)-O(5)	1.9833(15)
Pd(2)-O(13A)#2	1.9917(16)
Pd(2)-O(13A)	1.9917(16)
Pd(2)-O(15)	1.9881(15)
Pd(2)-O(15)#2	1.9881(15)
O(3A)#1-Pd(1)-O(3A)	180.0
O(5)#1-Pd(1)-O(3A)	85.40(6)
O(5)#1-Pd(1)-O(3A)#1	94.60(6)
O(5)-Pd(1)-O(3A)#1	85.40(6)
O(5)-Pd(1)-O(3A)	94.60(6)
O(5)#1-Pd(1)-O(5)	180.0
C(3)-O(3A)-Pd(1)	122.01(14)
C(5)-O(5)-Pd(1)	122.94(16)
O(13A)#2-Pd(2)-O(13A)	180.0
O(15)-Pd(2)-O(13A)	94.64(6)
O(15)-Pd(2)-O(13A)#2	85.36(6)
O(15)#2-Pd(2)-O(13A)#2	94.64(6)
O(15)#2-Pd(2)-O(13A)	85.36(6)
O(15)-Pd(2)-O(15)#2	180.0
C(13)-O(13A)-Pd(2)	122.04(14)
C(15)-O(15)-Pd(2)	122.60(16)

Symmetry transformations used to generate equivalent atoms:
#1 -x+1,-y+1,-z+1 #2 -x,-y+1,-z+2

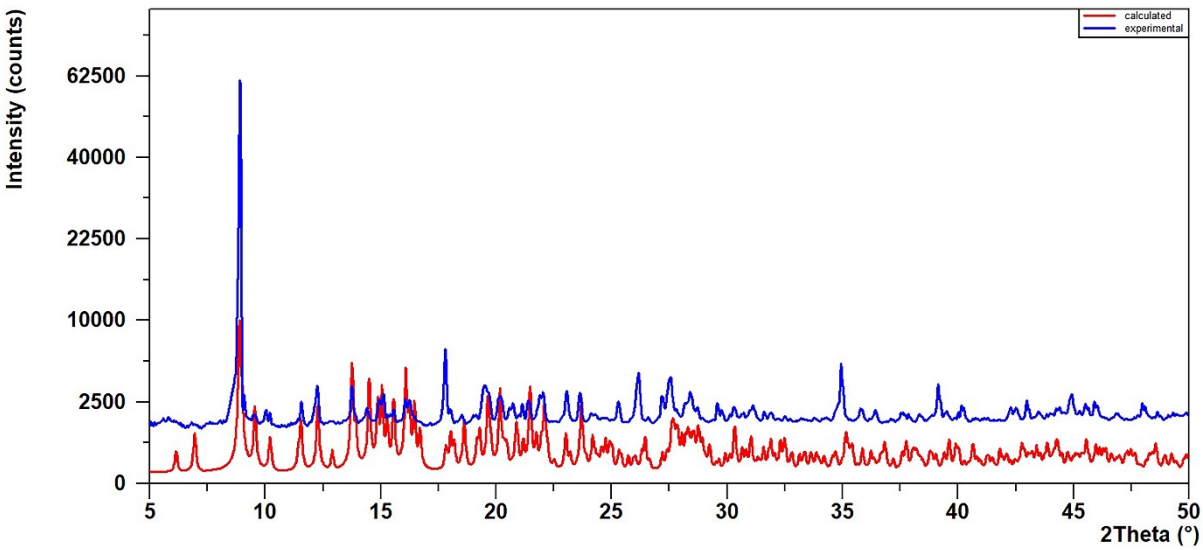

Figure S 1 Experimental (blue) and calculated (red) XRD patterns of the [Pd(tbaoac)$_2$] (**1**).

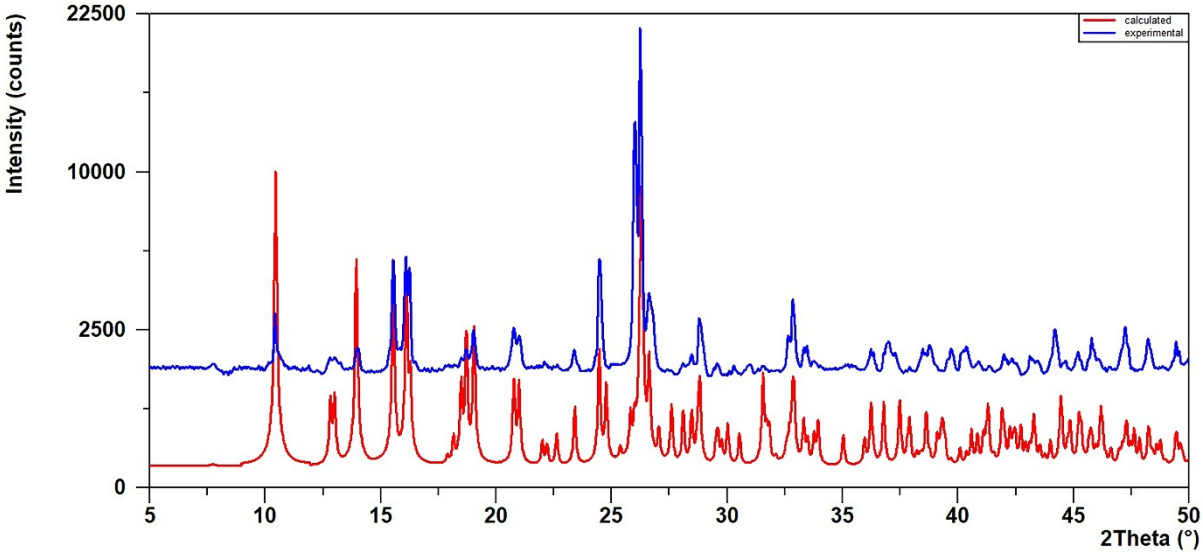

Figure S 2 Experimental (blue) and calculated (red) XRD patterns of the [Pd(ipaoac)$_2$] (**2**).

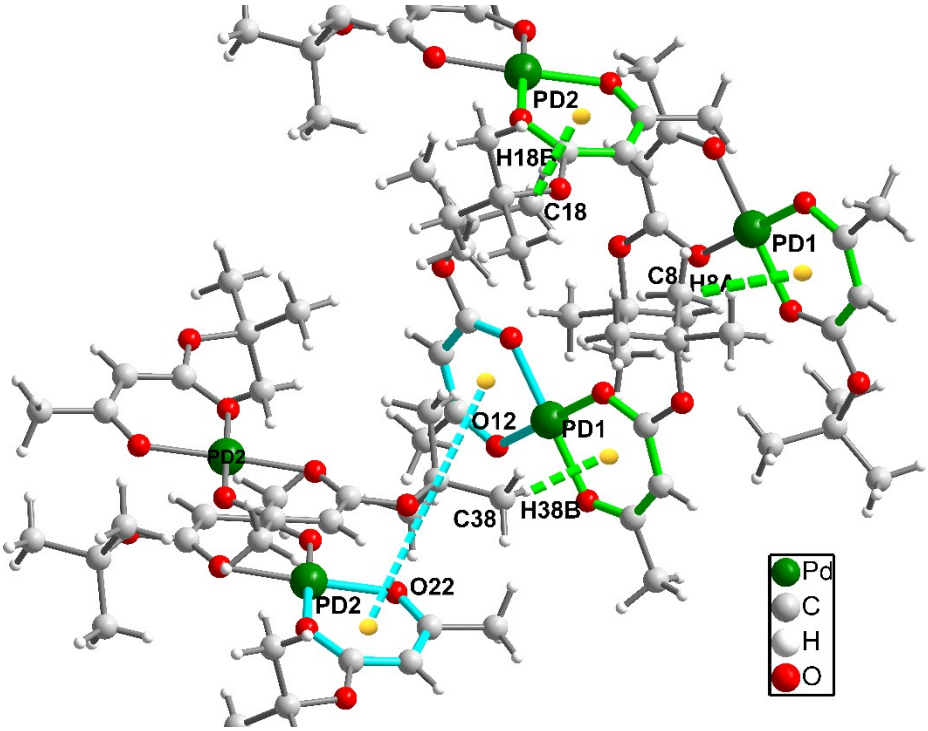

Figure S 3 C-H…π interactions between C8-H8, C23-H23, C38-H38, and chelate ring (green dashed lines) and between chelate rings (blue dashed lines) in the compound $[Pd(tbaoac)_2]$ (**1**).

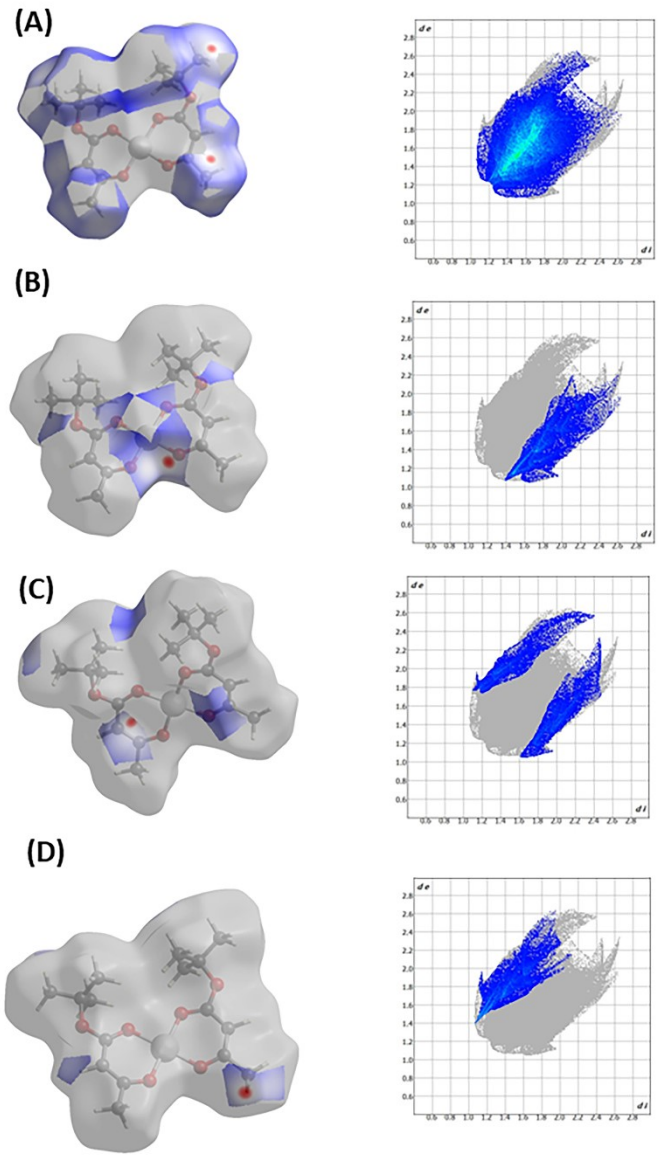

Figure S 4 Hirshfeld surfaces (left) and fingerprints (right) of selected interactions created in the crystal network of [Pd(tbaoac)$_2$] (**1**) for Pd2 molecule: (A) for H…H (63.5%), (B) for O…H (11.2%), (C) for C…H and H…C (11.1%), and (D) for H…O (10.0%). In brackets, there is a given surface area included as a percentage of the total surface area.

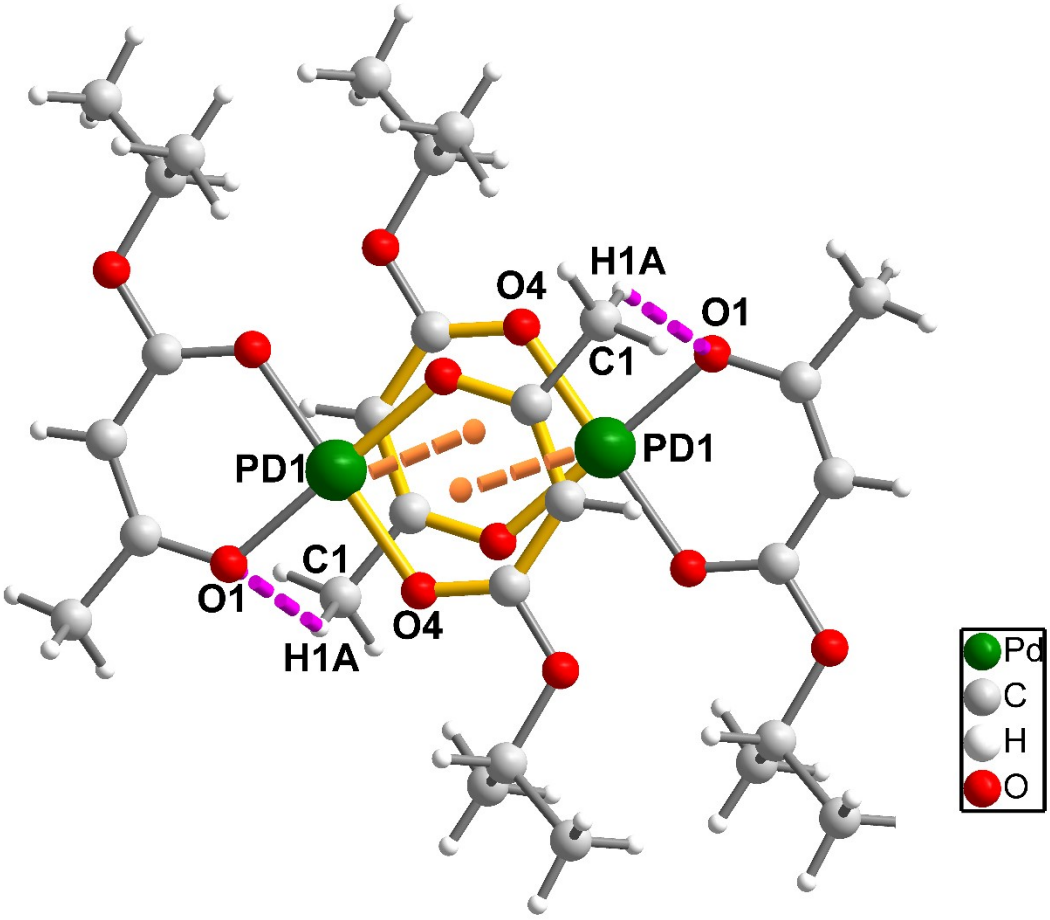

Figure S 5 π–π interactions between palladium ion and chelate ring (orange dashed lines) and O…H hydrogen bonds (magenta dashed lines) in the compound [Pd(ipaoac)$_2$] (**2**).

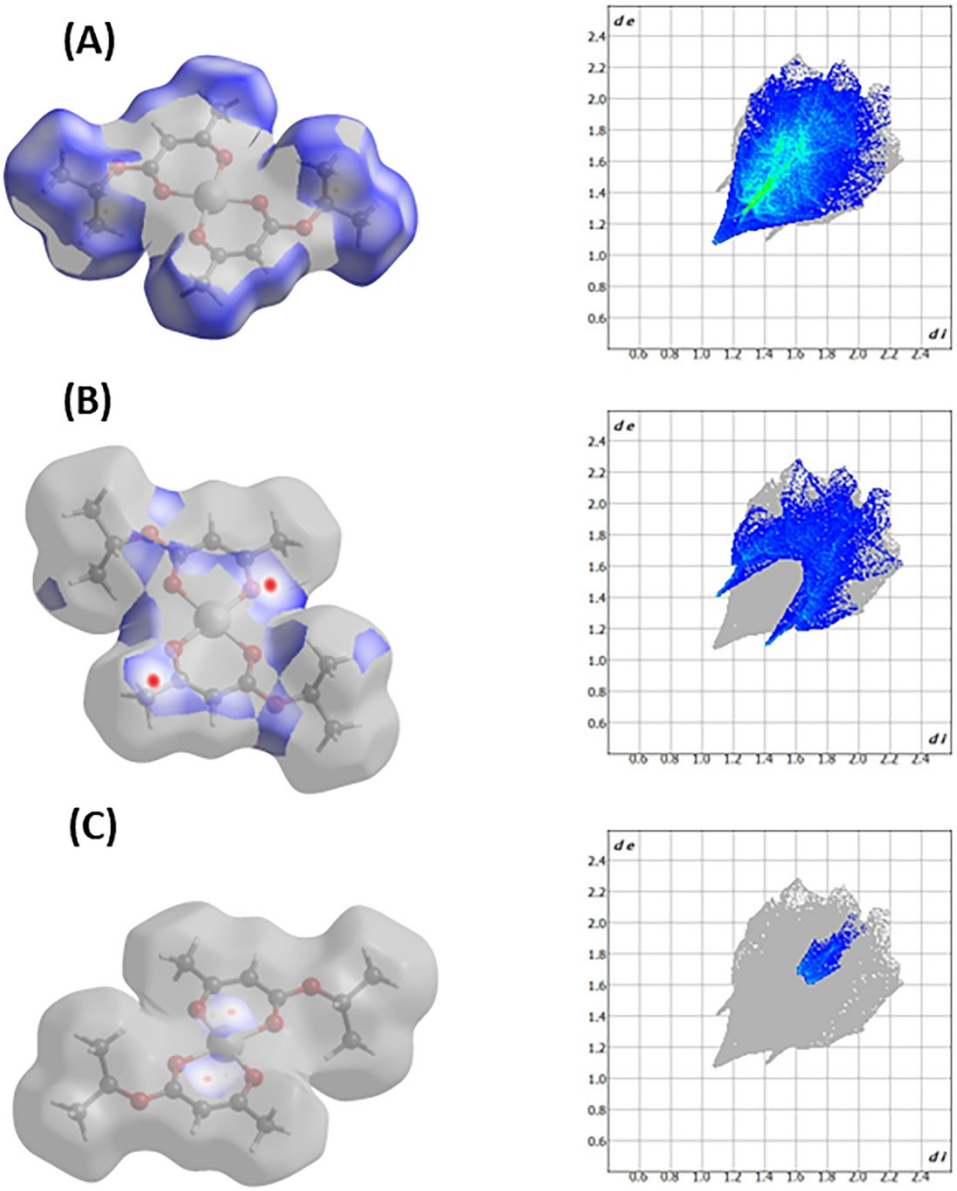

Figure S 6 Hirshfeld surfaces (left) and fingerprints (right) of selected interactions created in the crystal network of [Pd(ipaoac)$_2$] (**2**): (A) for H…H (67.0%), (B) for H…O (18.1%), and (C) for C…Pd (3.5%). In brackets, there is a given surface area included as a percentage of the total surface area.

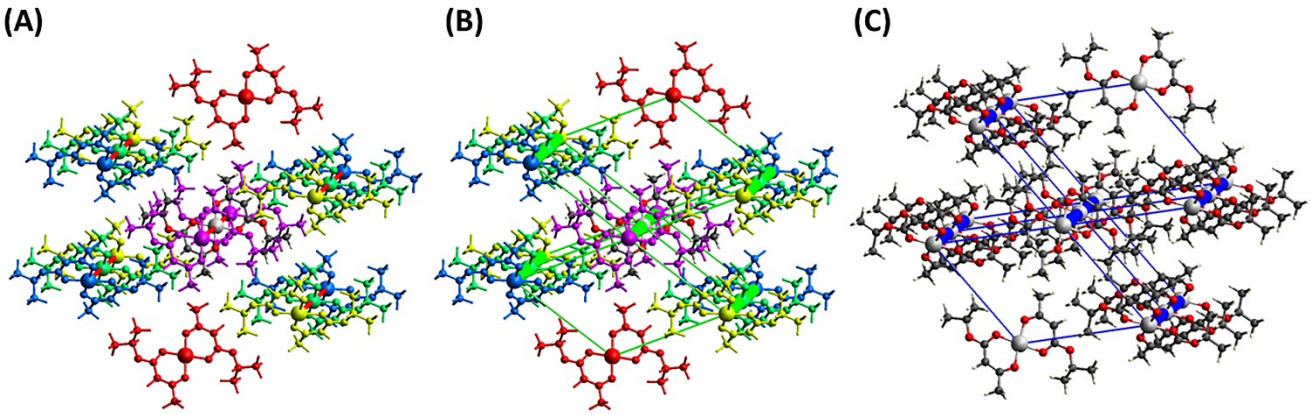

Figure S 7 Interactions energy: (A) – electrostatic, (B) – van der Waals, and (C) – total in the crystal network of [Pd(ipaoac)$_2$] (**2**).

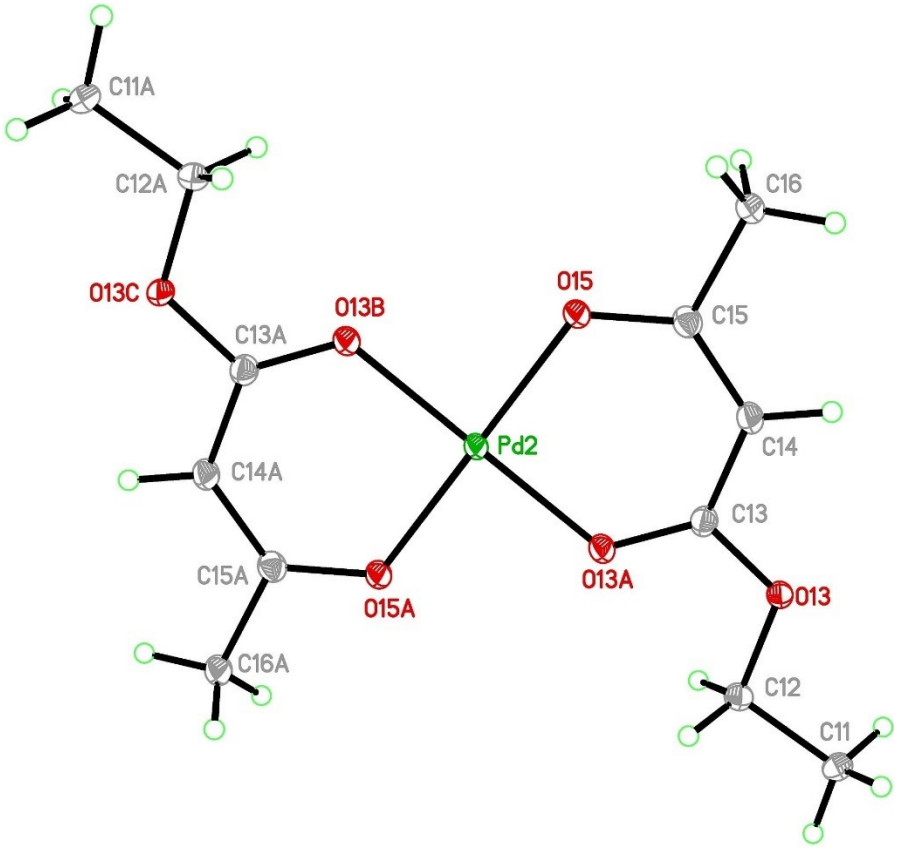

Figure S 8 The structure of [Pd(eaoac)$_2$] (**3**) with the numbering scheme.

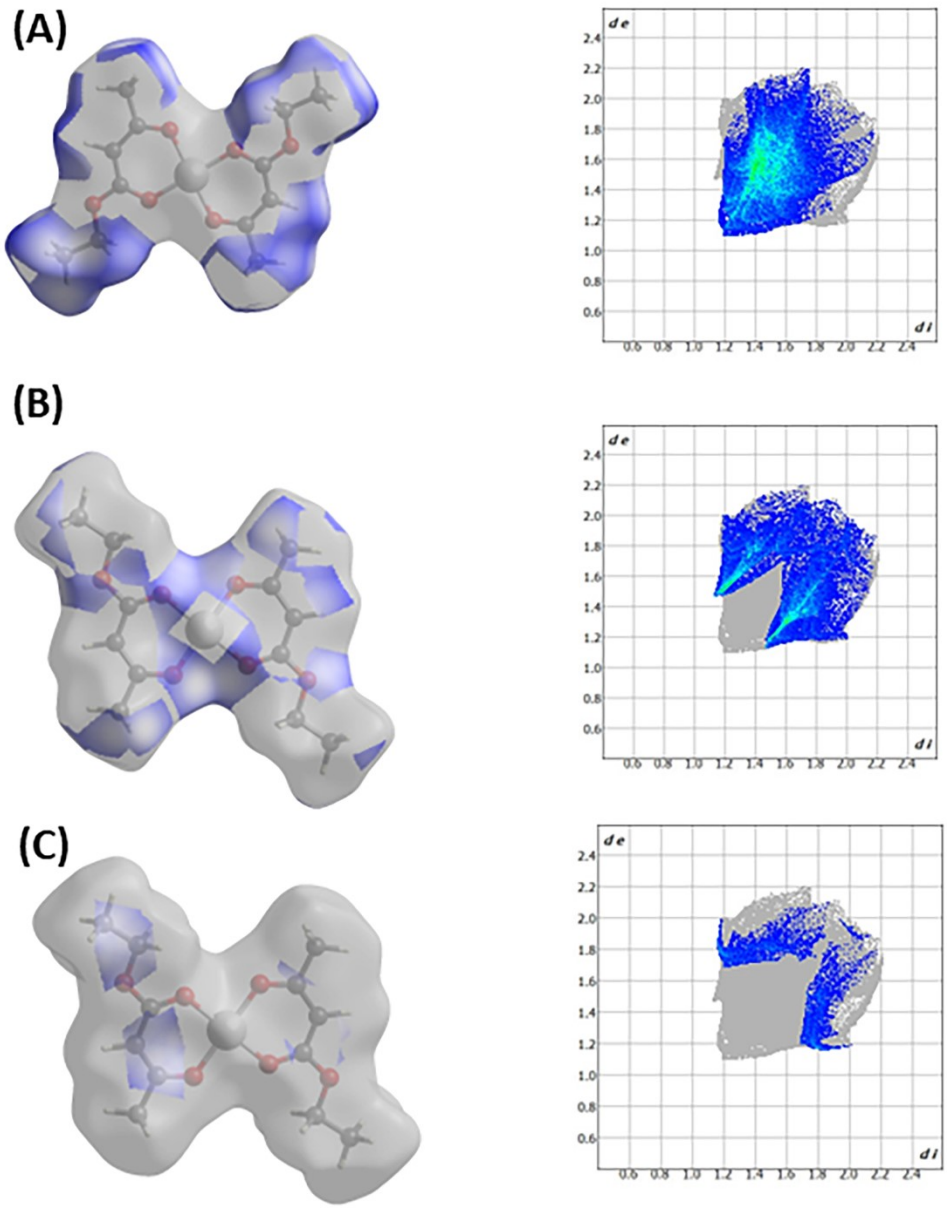

Figure S 9 Hirshfeld surfaces (left) and fingerprints (right) of selected interactions created in the crystal network of [Pd(eaoac)$_2$] (**3**) for Pd1 molecule: (A) for H…H (53.1%), (B) for O…H (29.7%), and (C) for C…H (7.4%). In brackets, there is a given surface area included as a percentage of the total surface area.

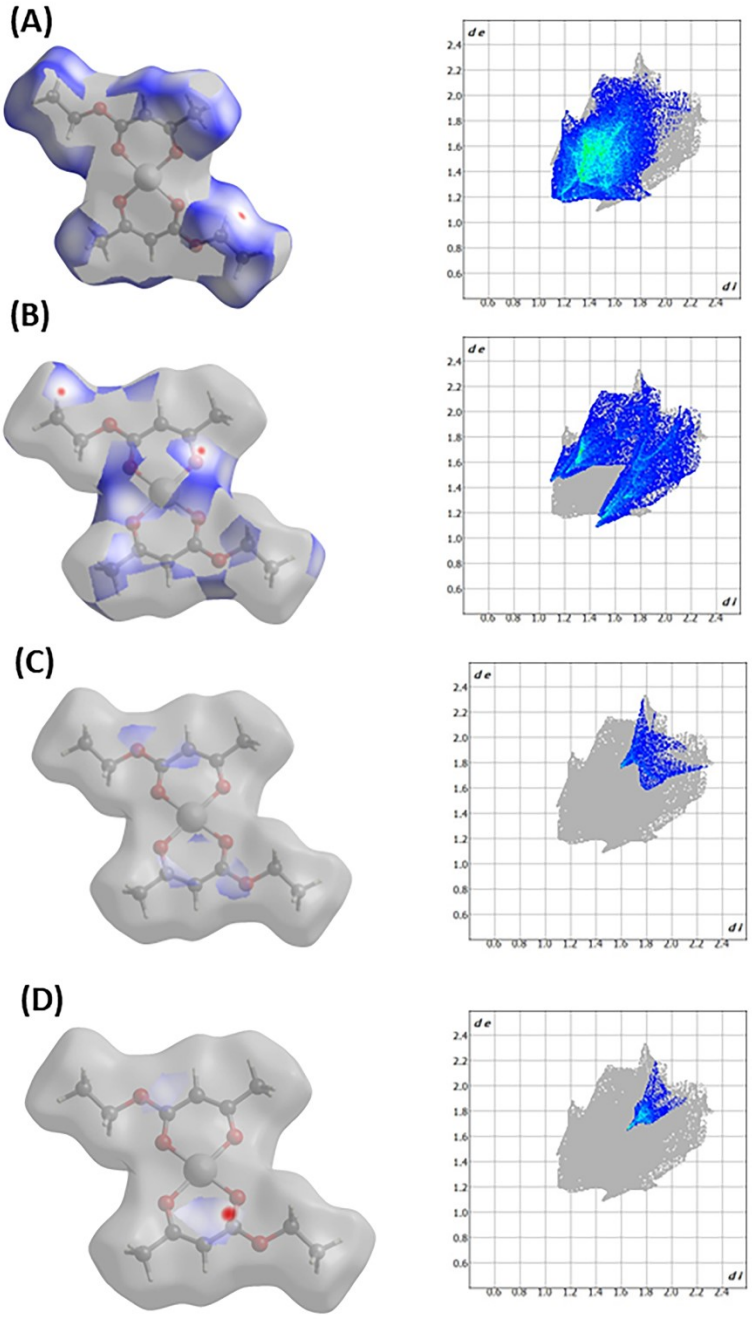

Figure S 10 Hirshfeld surfaces (left) and fingerprints (right) of selected interactions created in the crystal network of [Pd(eaoac)$_2$] (**3**) for Pd2 molecule: (A) for H…H (58.1%), (B) for H…O (25.9%), (C) for C…O (4.0%), and (D) for C…C (3.6%). In brackets, there is a given surface area included as a percentage of the total surface area.

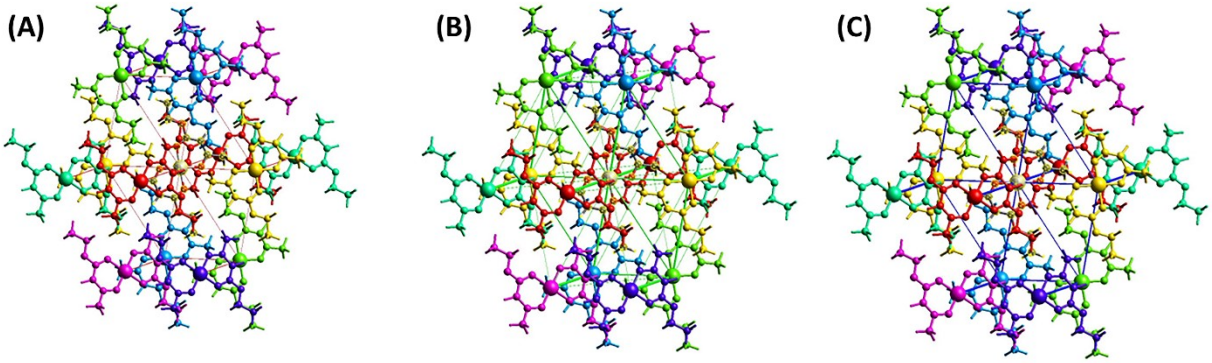

Figure S 11 Interactions energy: (A) – electrostatic, (B) – van der Waals, and (C) – total in the crystal network of [Pd(eaoac)$_2$] (**3**) for Pd1 molecule.

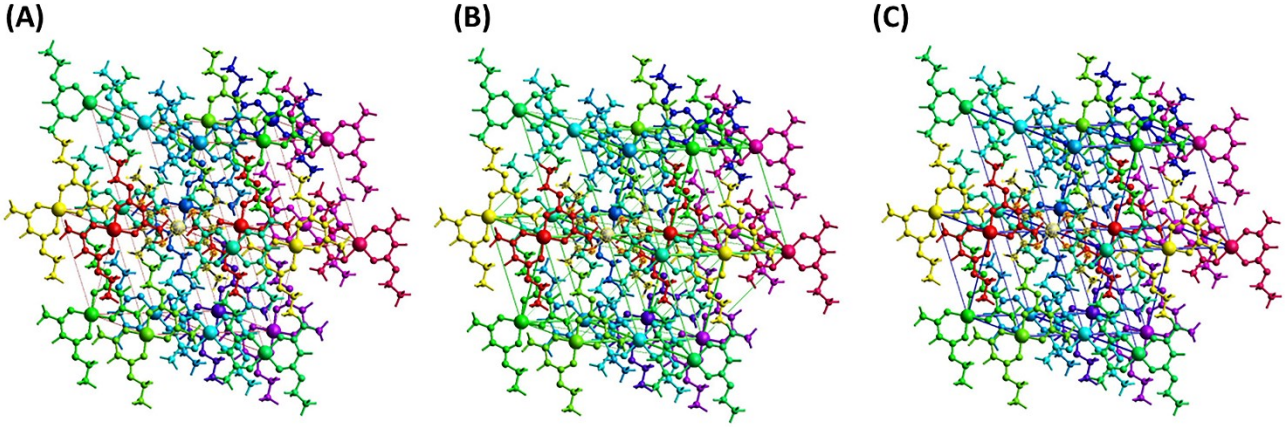

Figure S 12 Interactions energy: (A) – electrostatic, (B) – van der Waals, and (C) – total in the crystal network of [Pd(eaoac)$_2$] (**3**) for Pd2 molecule.

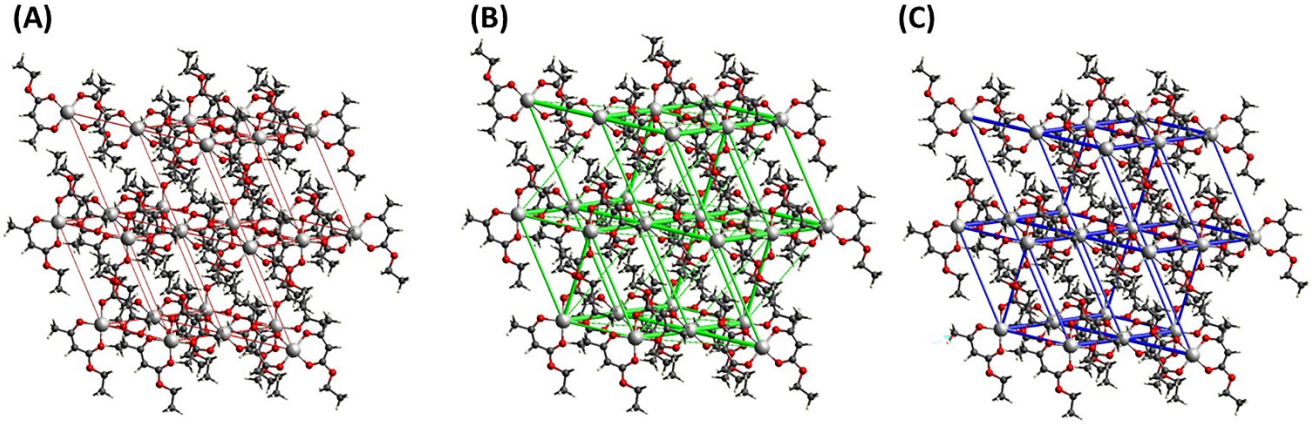

Figure S 13 Interactions energy: (A) – electrostatic, (B) – van der Waals, and (C) – total in the crystal network of [Pd(eaoac)$_2$] (**3**) for Pd1 and Pd2 molecules.

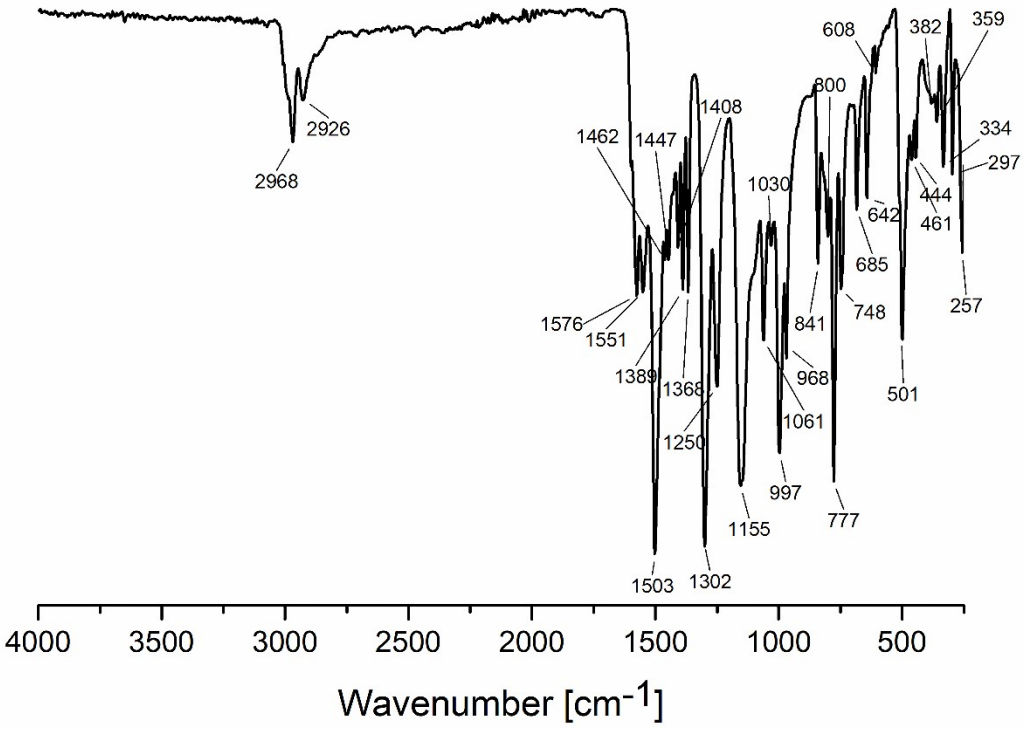

Figure S 14 ATR-IR spectrum for the compound [Pd(tbaoac)$_2$] (**1**).

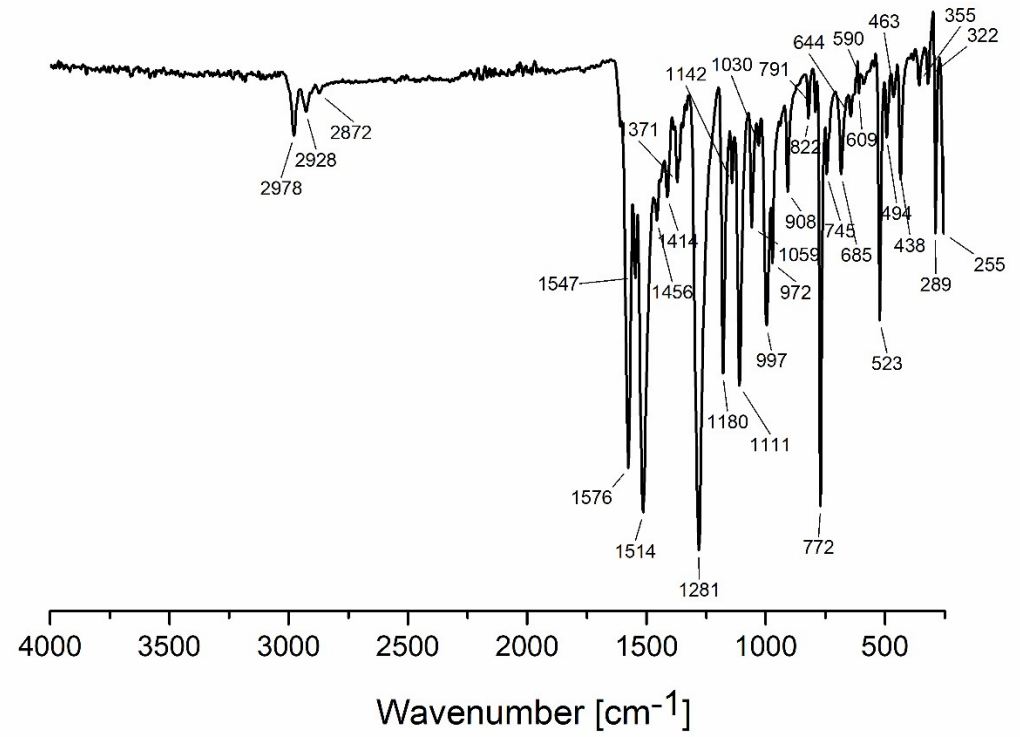

Figure S 15 ATR-IR spectrum for the compound [Pd(ipaoac)$_2$] (**2**).

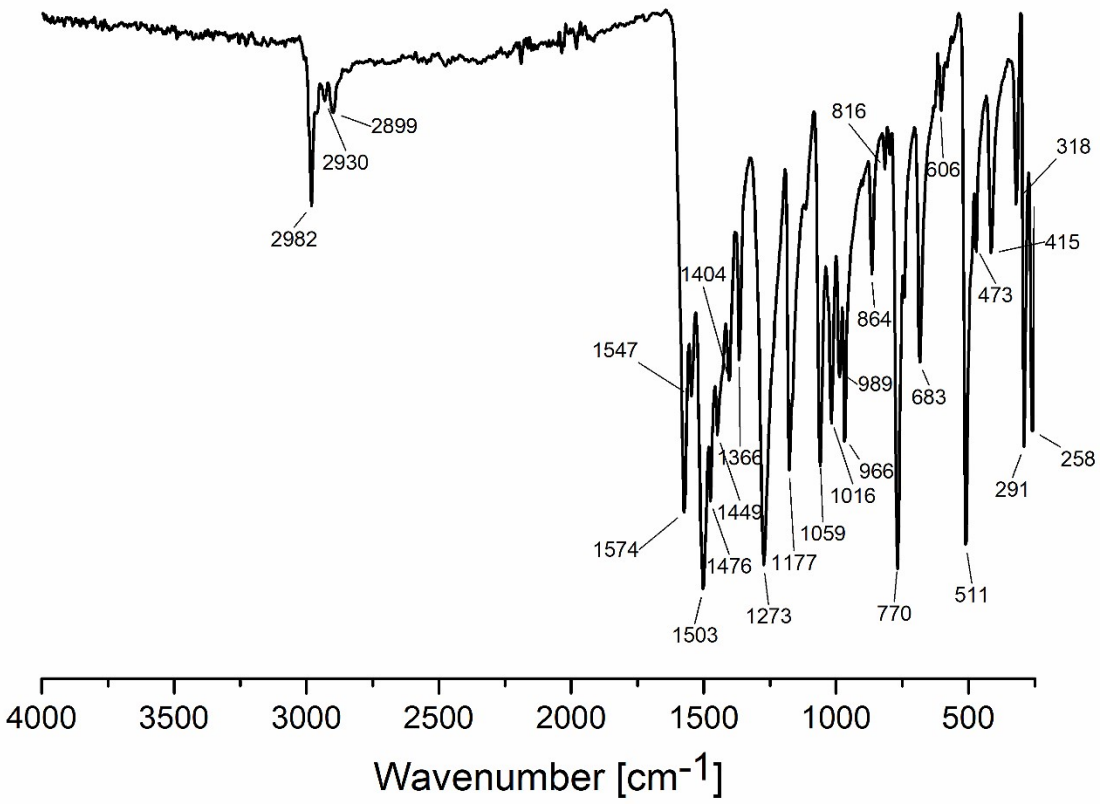

Figure S 16 ATR-IR spectrum for the compound [Pd(eaoac)$_2$] (**3**).

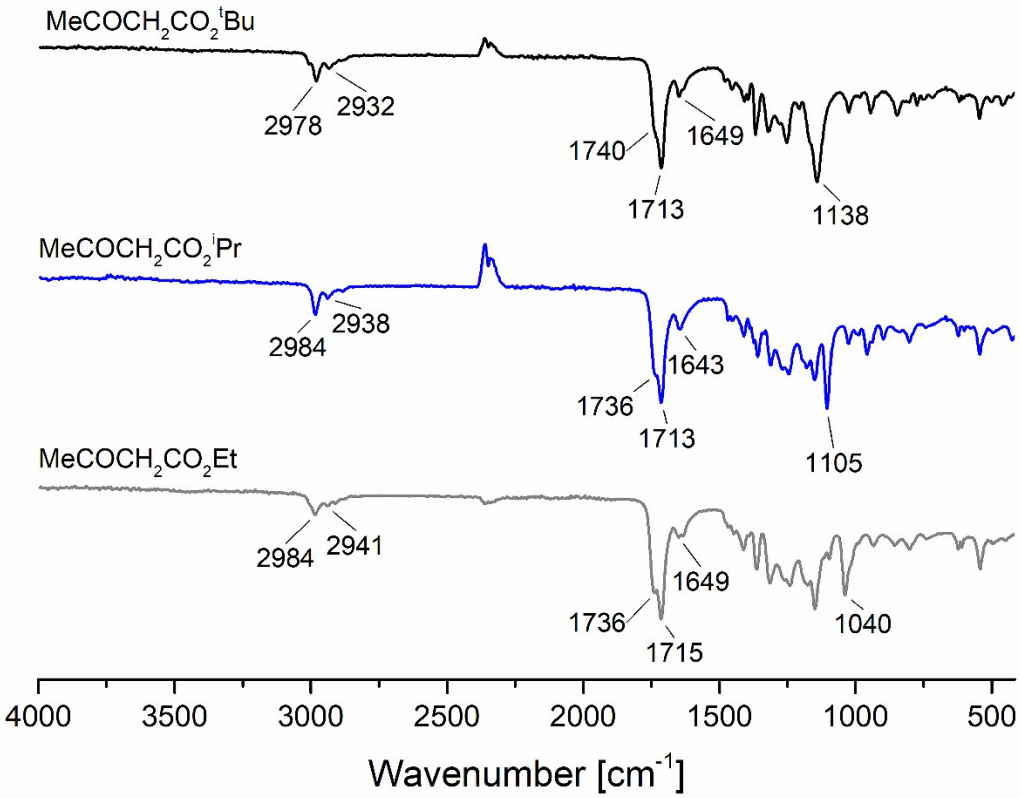

Figure S 17 ATR-IR spectra for the protonated ligands: MeCOCH$_2$CO$_2$^{t}Bu – tbaoacH (black), MeCOCH$_2$CO$_2$^{i}Pr – ipaoacH (blue), and MeCOCH$_2$CO$_2$Et – eaoacH (grey).

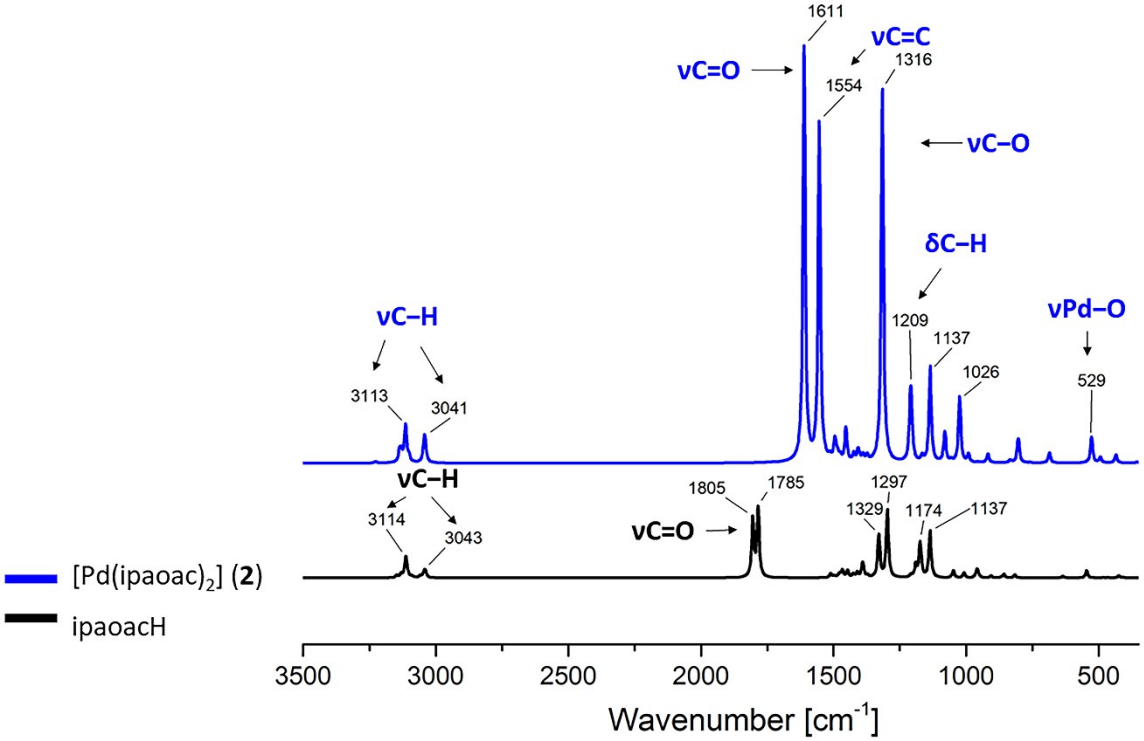

Figure S 18 Theoretical infrared spectra calculated by DFT B3LYP-D3/def2-TZVPP for the compound [Pd(ipaoac)$_2$] (**2**) (blue line) and ligand ipaoacH (black line).

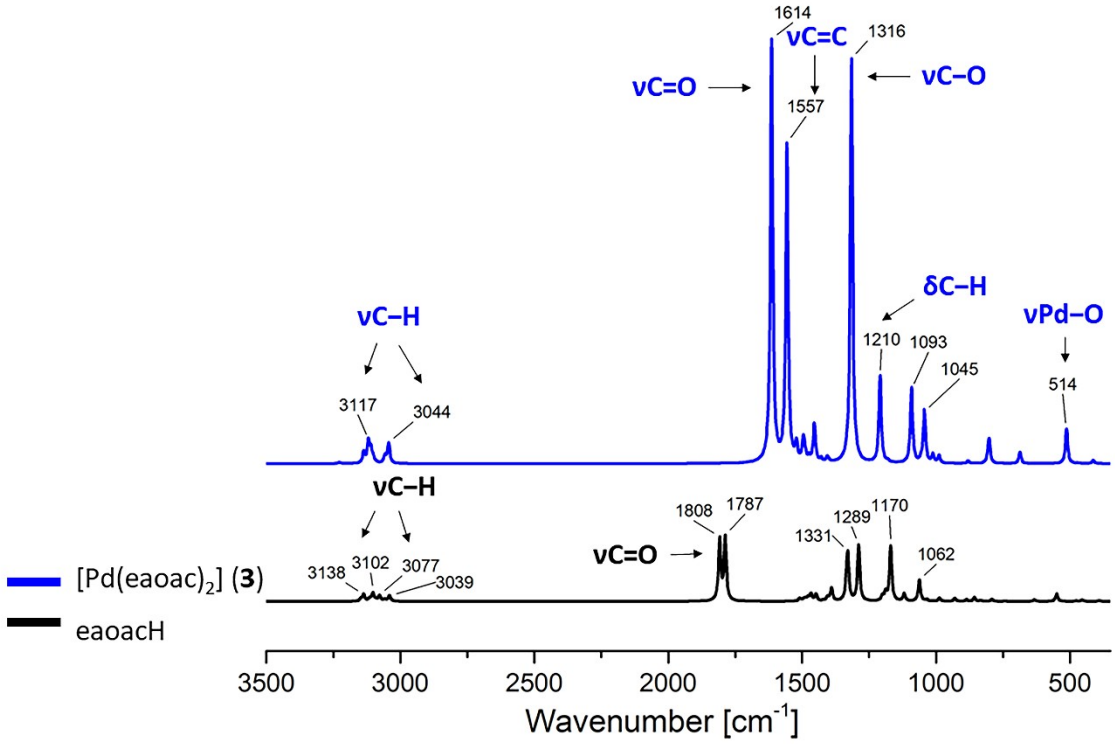

Figure S 19 Theoretical infrared spectra calculated by DFT B3LYP-D3/def2-TZVPP for the compound [Pd(eaoac)$_2$] (**3**) (blue line) and ligand eaoacH (black line).

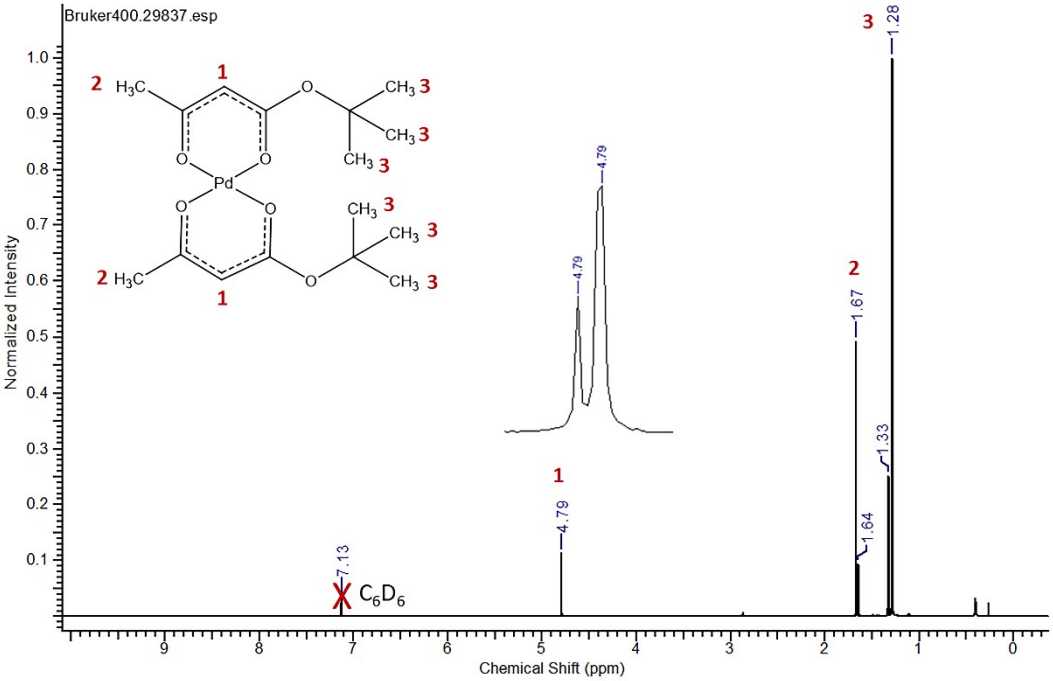

Figure S 20 ^{1}H NMR spectrum of the compound [Pd(tbaoac)$_2$] (**1**).

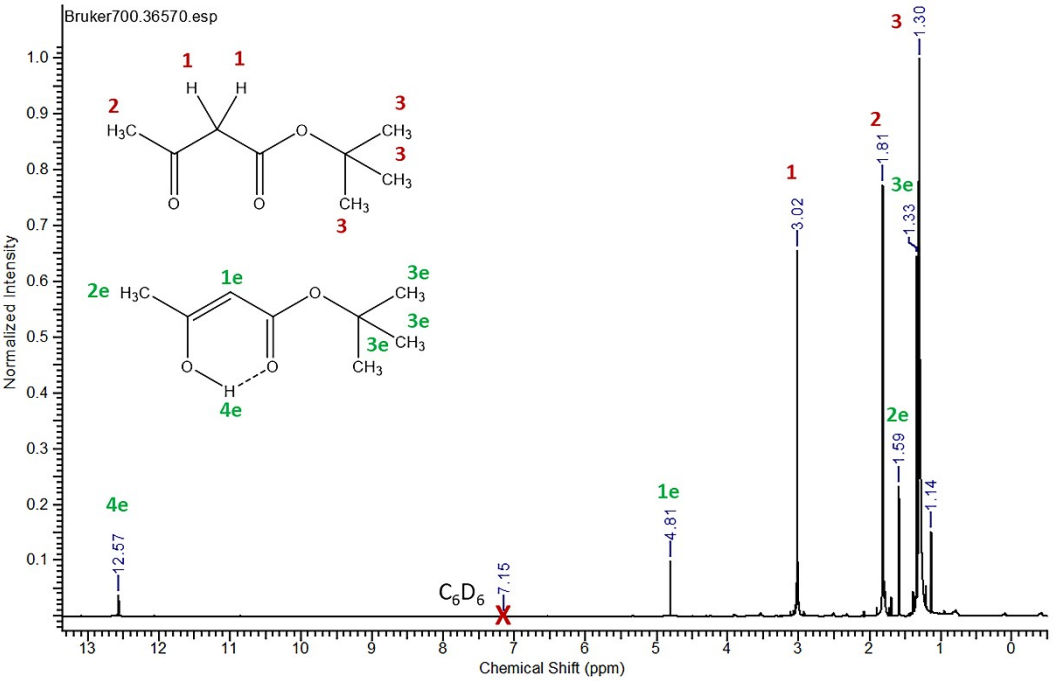

Figure S 21 ^{1}H NMR spectrum of the tbaoacH – $MeCOCH_2CO_2{}^{t}Bu$.

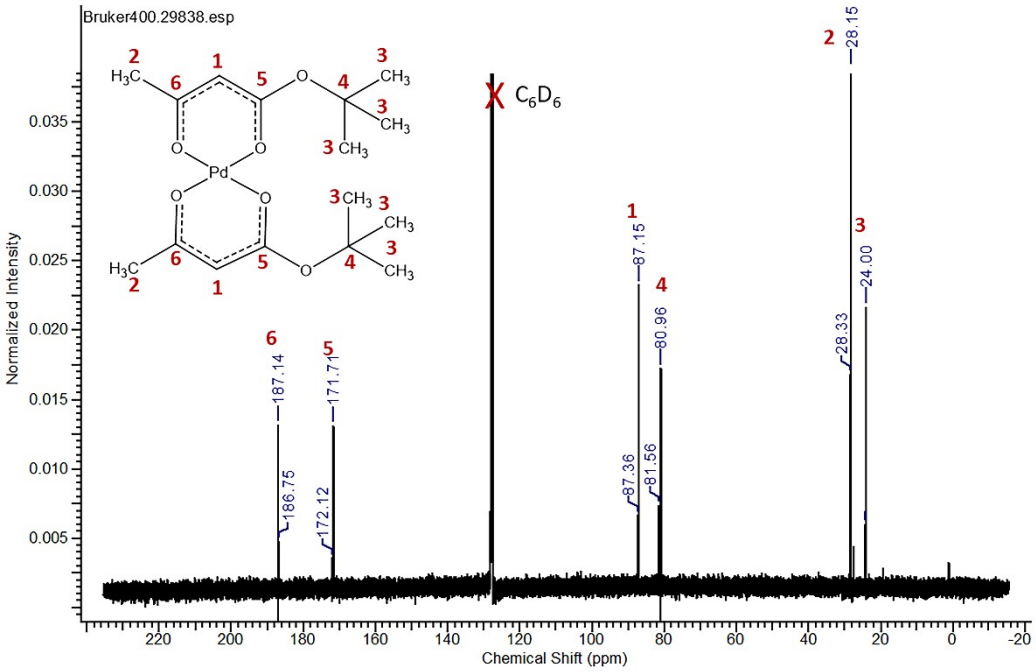

Figure S 22 ^{13}C NMR spectrum of the compound [Pd(tbaoac)$_2$] (**1**).

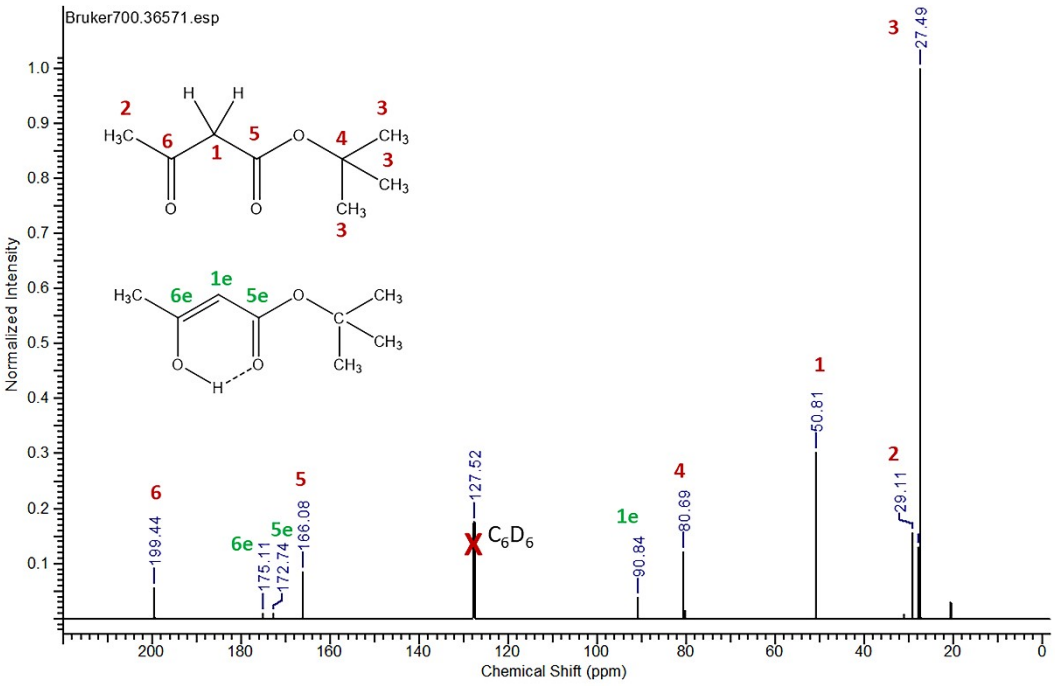

Figure S 23 ^{13}C NMR spectrum of the tbaoacH – $MeCOCH_2CO_2{}^tBu$.

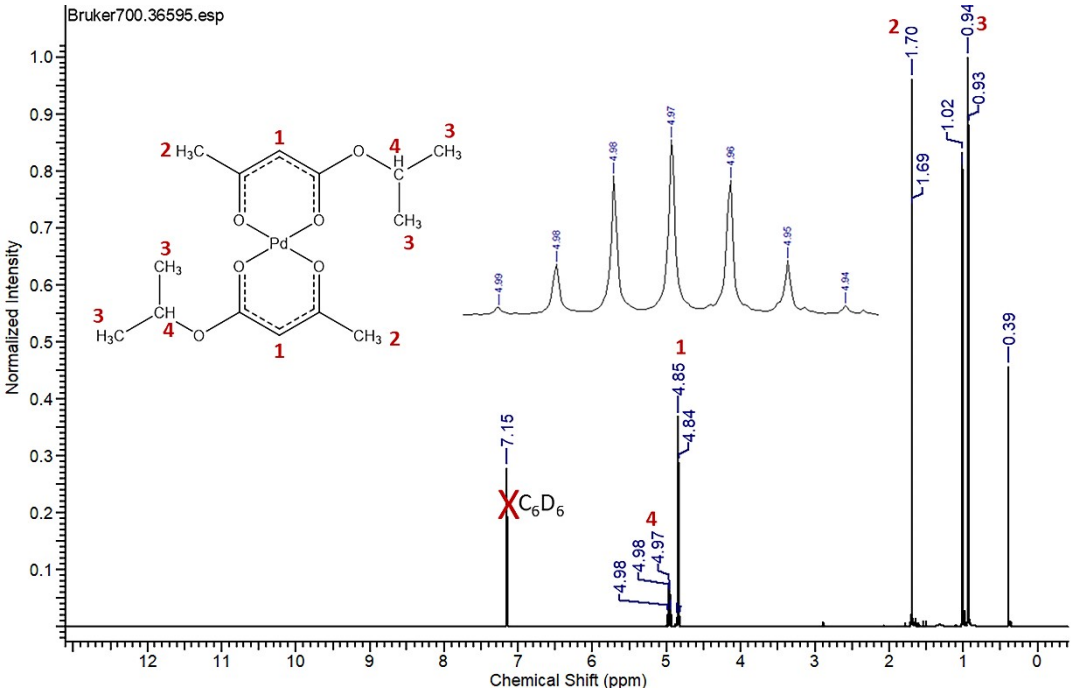

Figure S 24 ^{1}H NMR spectrum of the compound [Pd(ipaoac)$_2$] (**2**).

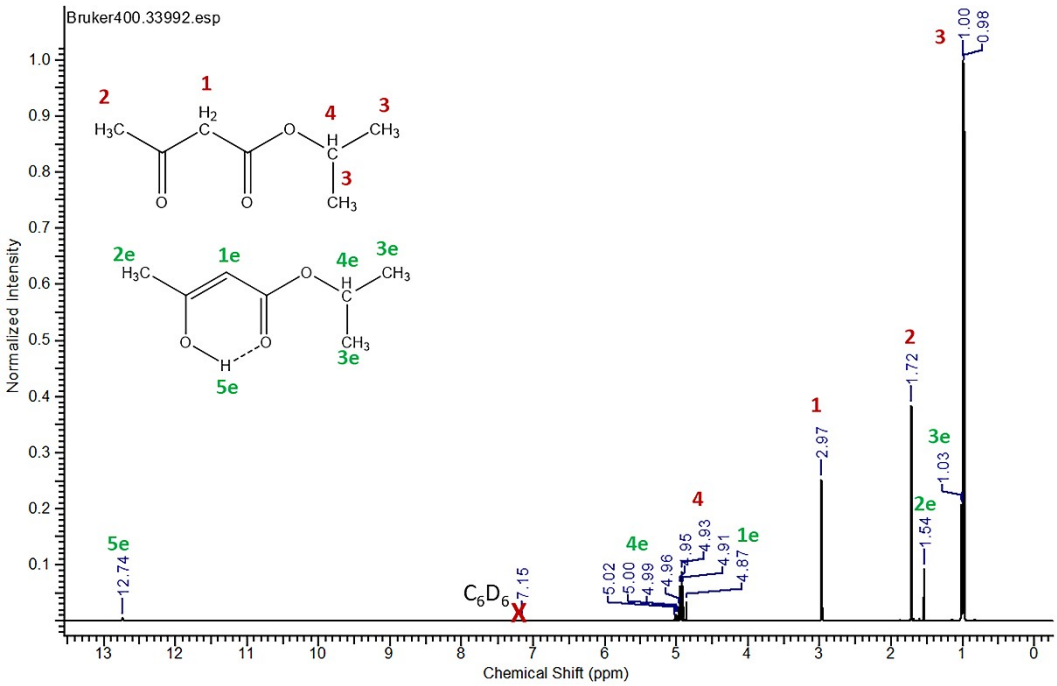

Figure S 25 ^{1}H NMR spectrum of the ipaoacH – MeCOCH$_2$CO$_2$^{i}Pr.

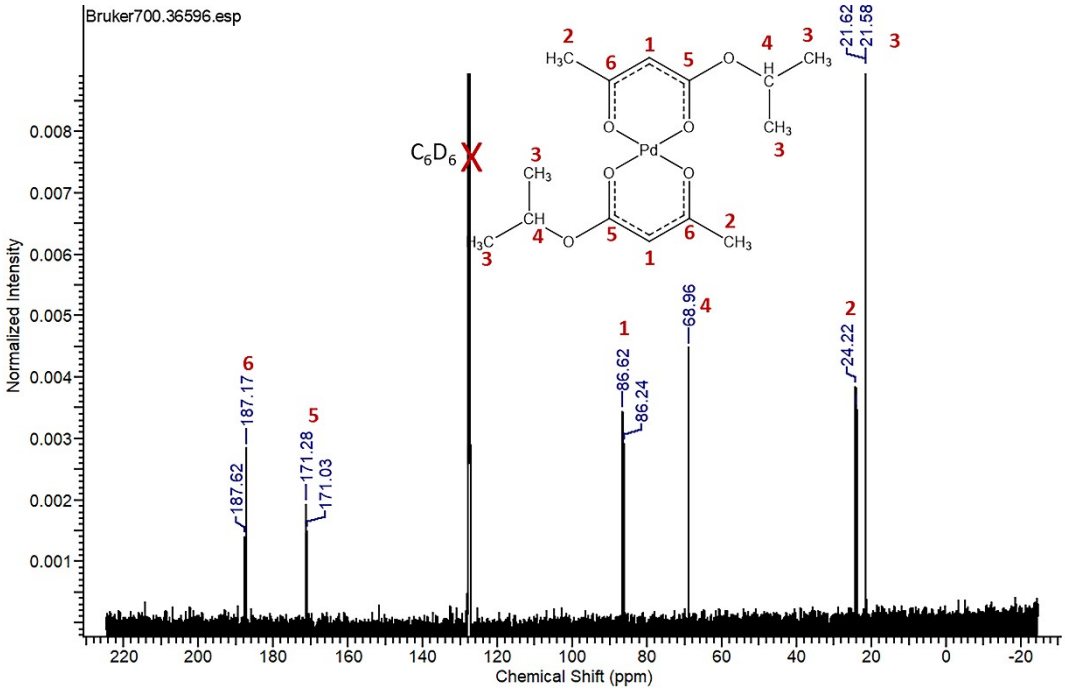

Figure S 26 ^{13}C NMR spectrum of the compound [Pd(ipaoac)$_2$] (**2**).

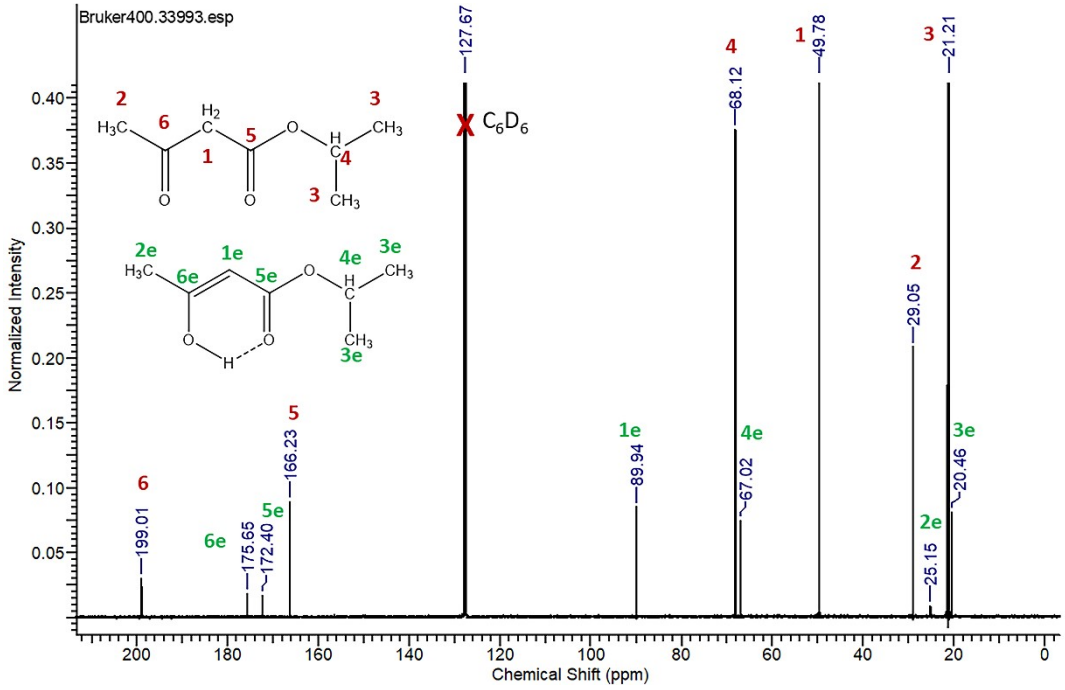

Figure S 27 ^{13}C NMR spectrum of the ipaoacH – MeCOCH$_2$CO$_2$^{i}Pr.

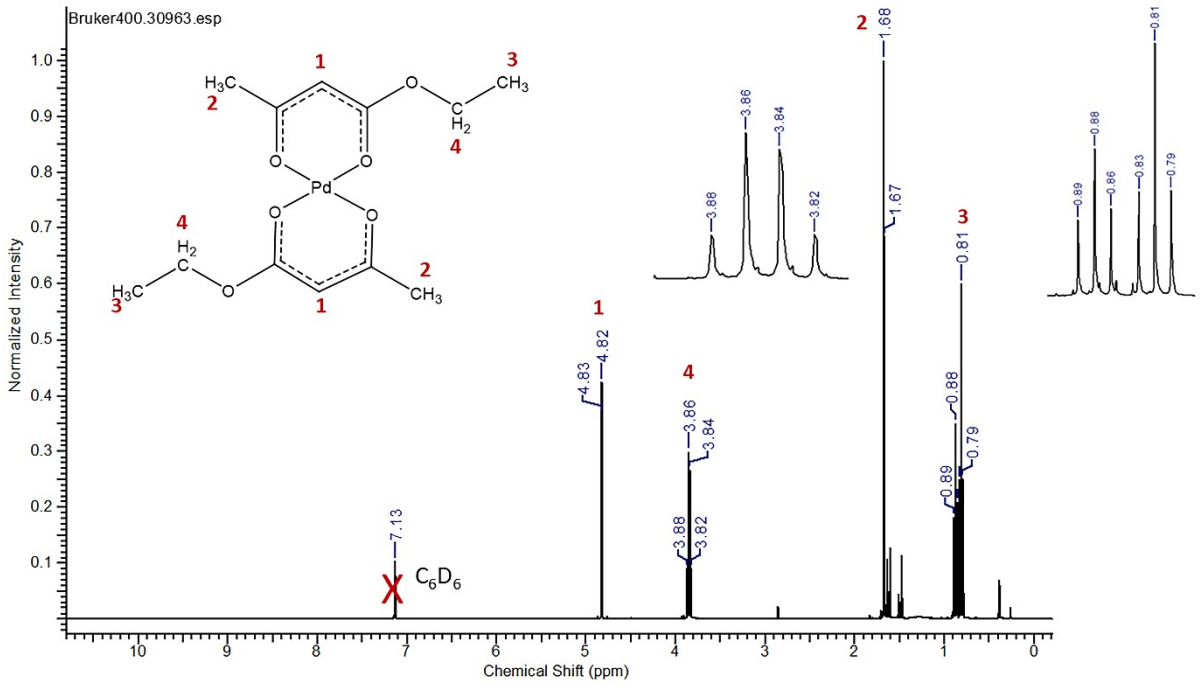

Figure S 28 ^{1}H NMR spectrum of the compound [Pd(eaoac)$_2$] (**3**).

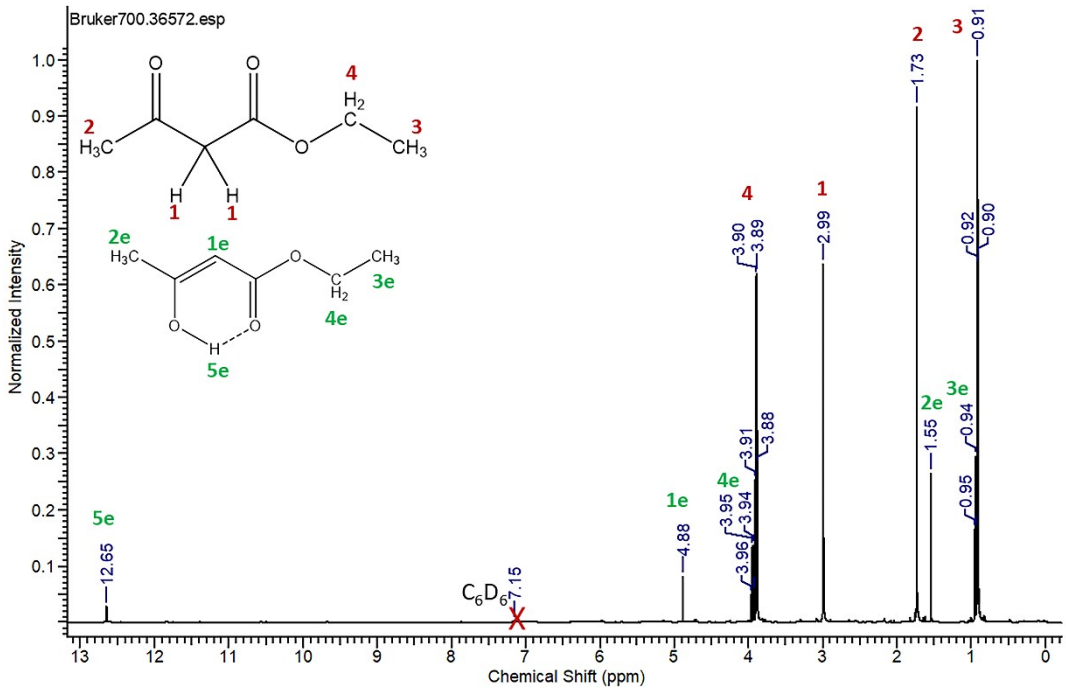

Figure S 29 ^{1}H NMR spectrum of the compound eaoacH – MeCOCH$_2$CO$_2$Et.

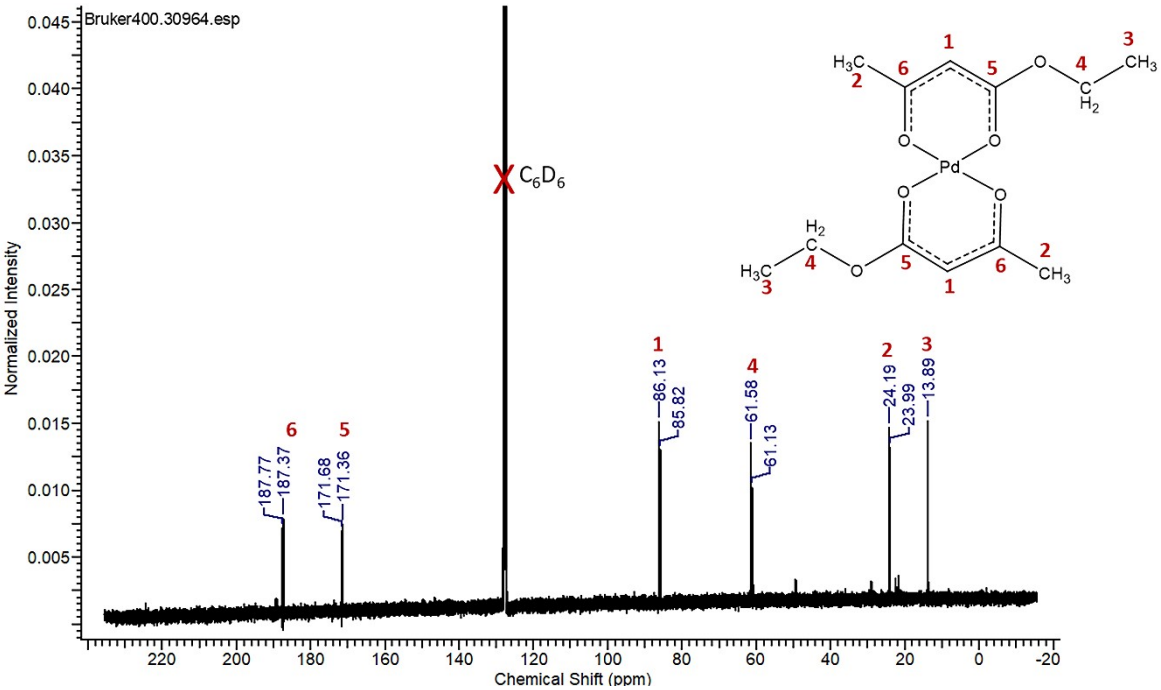

Figure S 30 ^{13}C NMR spectrum of the compound [Pd(eaoac)$_2$] (**3**).

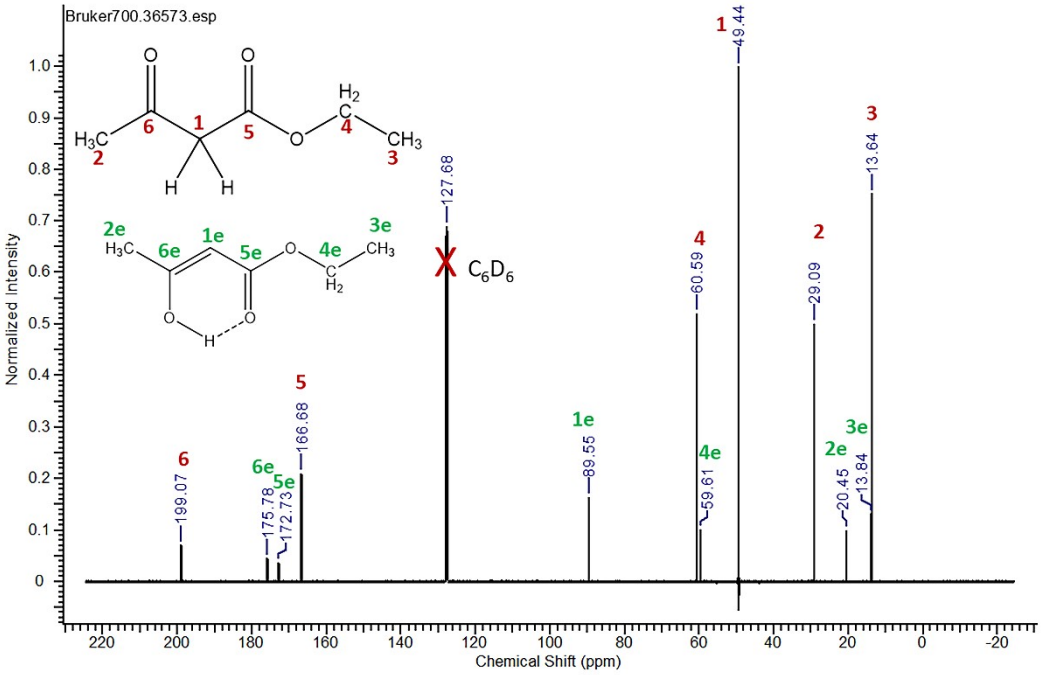

Figure S 31 ^{13}C NMR spectrum of the eaoacH – MeCOCH$_2$CO$_2$Et.

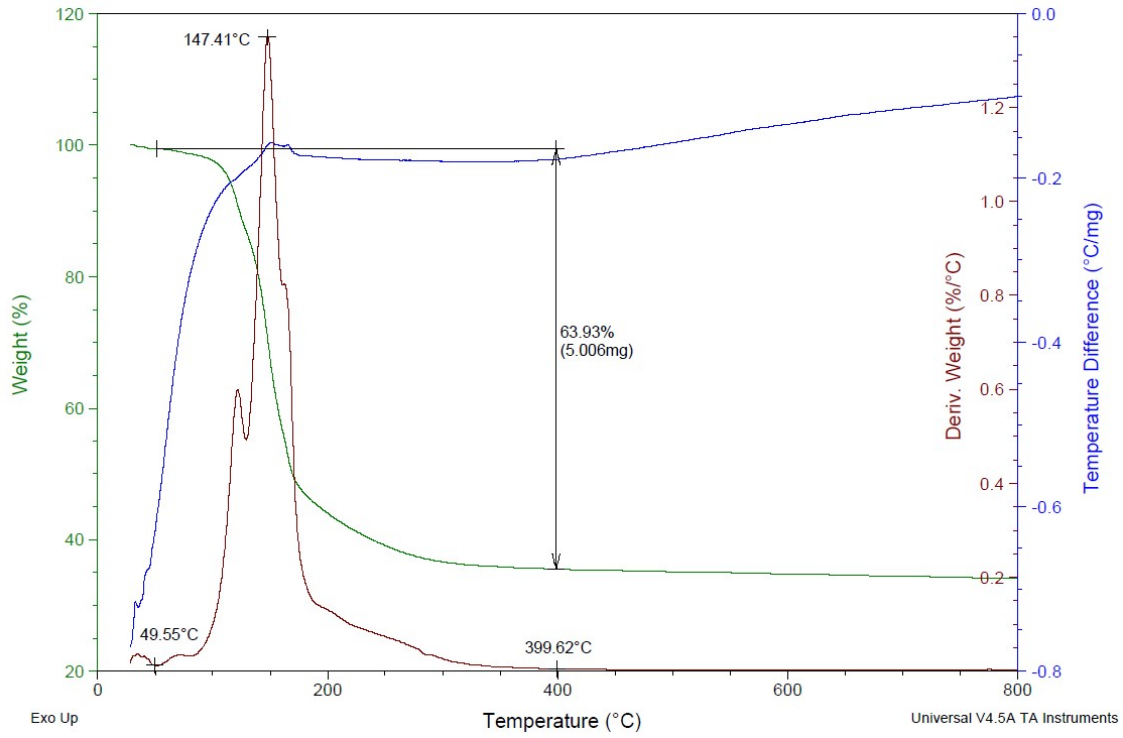

Figure S 32 Thermogram of [Pd(ipaoac)$_2$] (**2**) (TG, DTG, DTA curves).

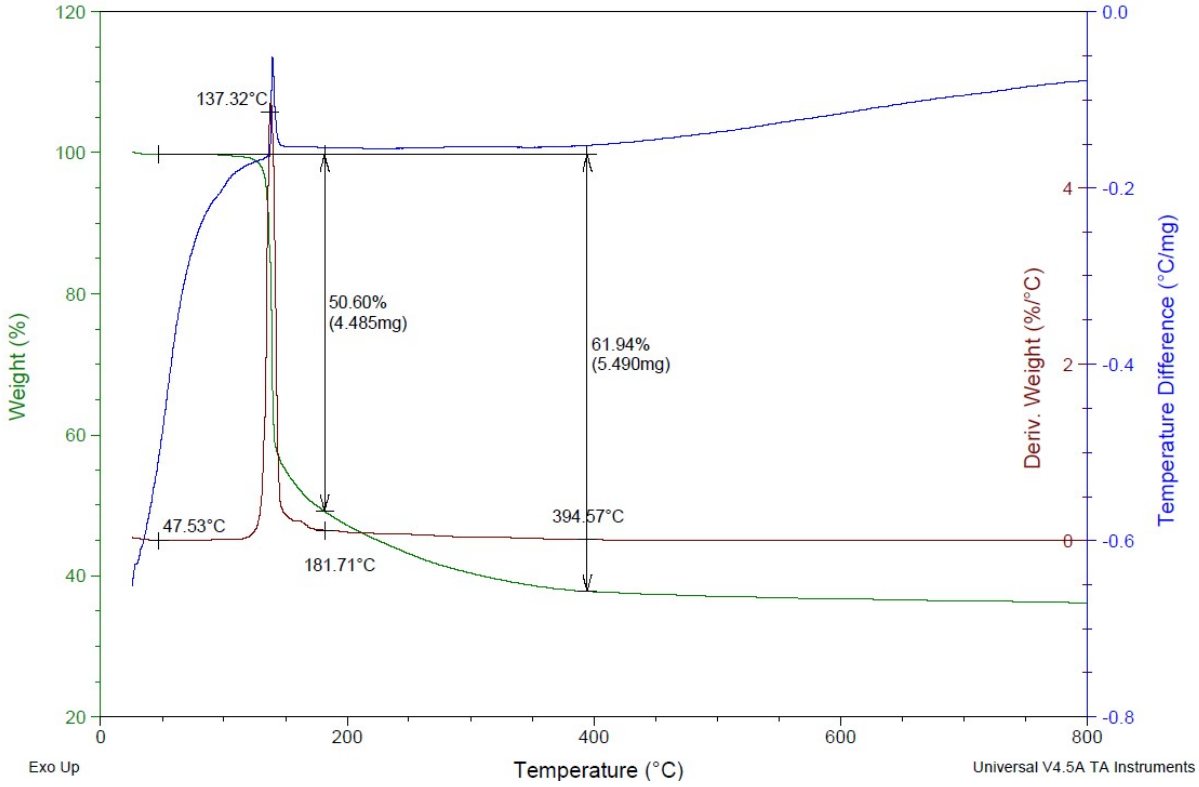

Figure S 33 Thermogram of [Pd(eaoac)$_2$] (**3**) (TG, DTG, DTA curves).

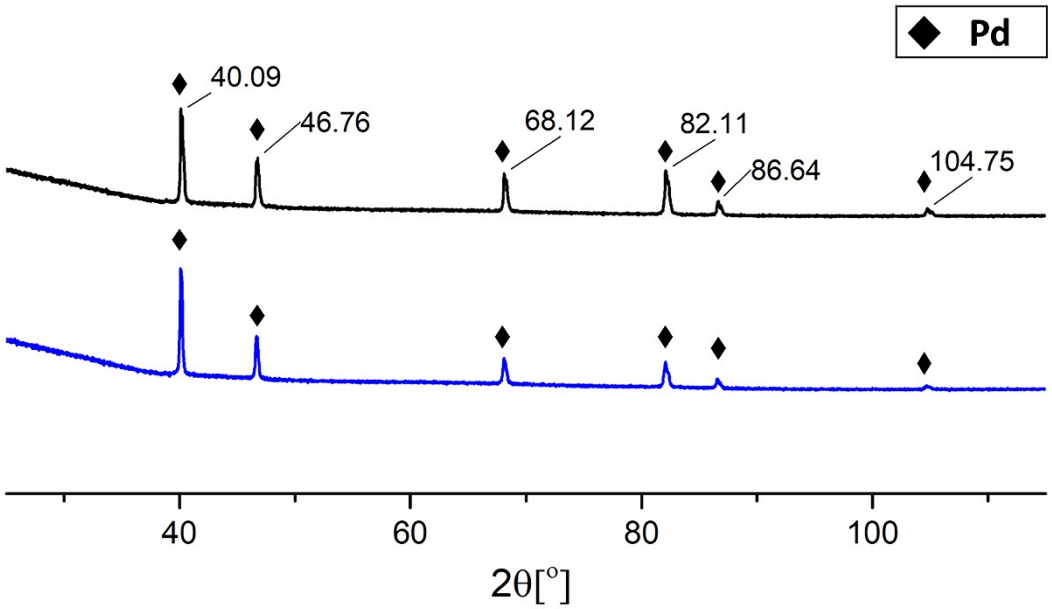

Figure S 34 XRD analysis of the residue after thermal analysis of [Pd(ipaoac)$_2$] (**2**) and [Pd(eaoac)$_2$] (**3**).

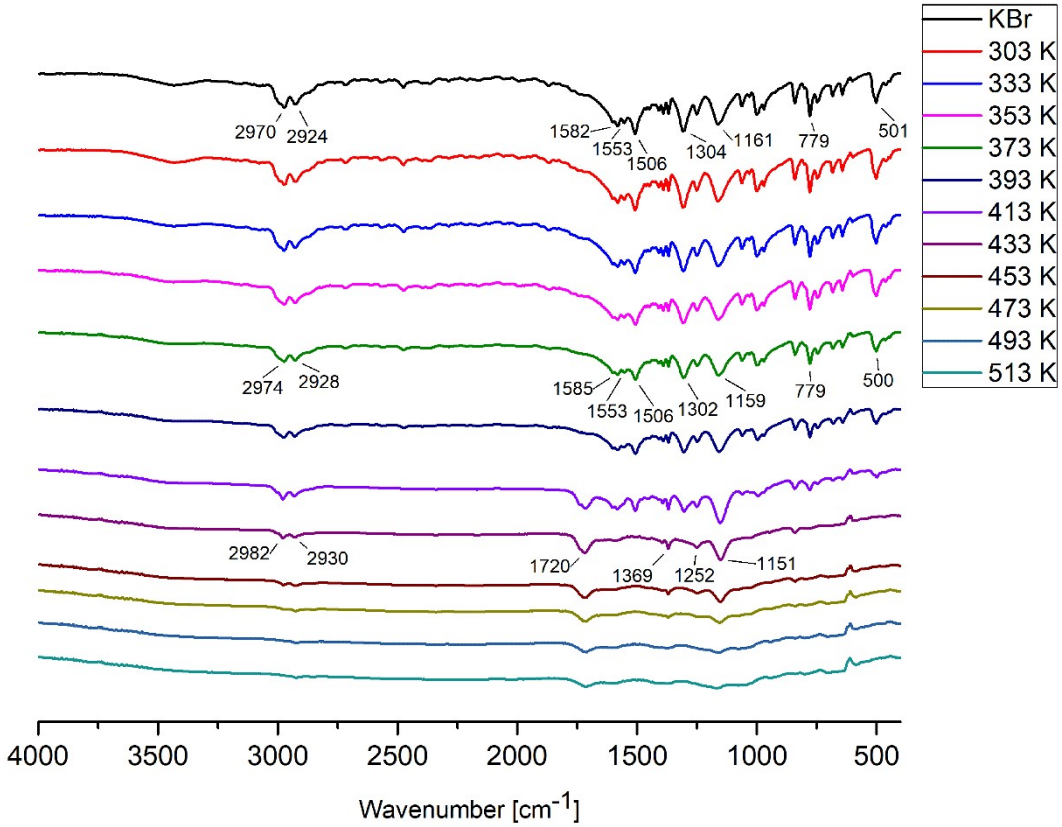

Figure S 35 VT IR spectra in the solid state for the compound [Pd(tbaoac)$_2$] (**1**) in the temperature range 303−513 K.

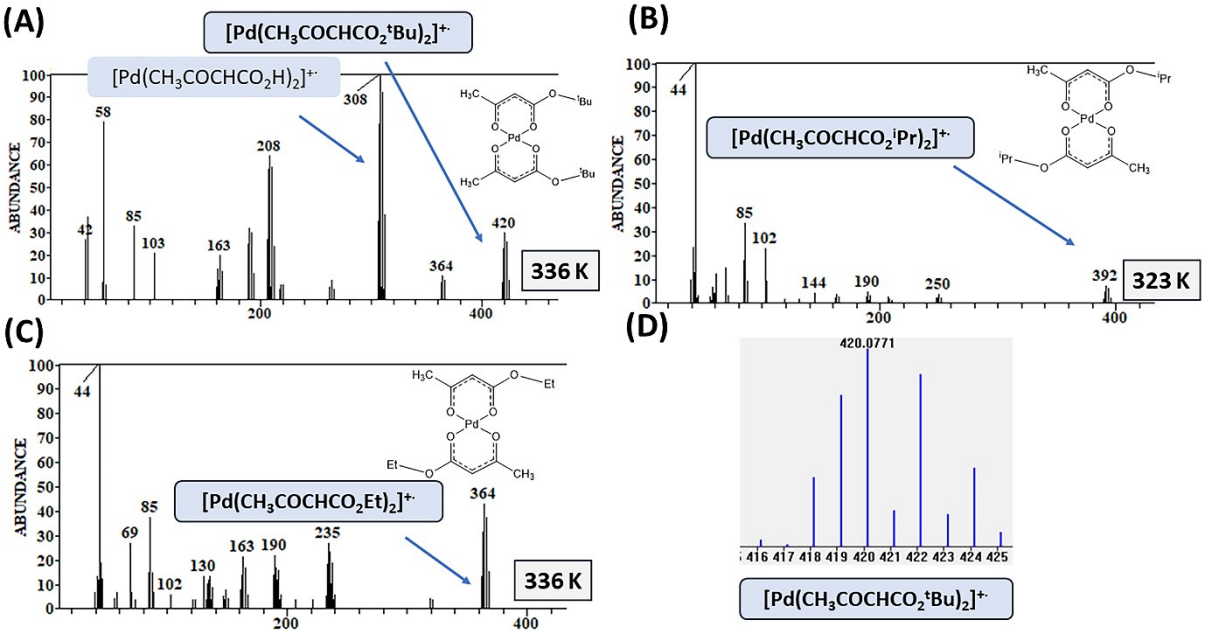

Figure S 36 EI MS spectra, where the molecular ions appeared: (A) − [Pd(tbaoac)$_2$] (**1**) at the temperature 336 K, (B) − [Pd(ipaoac)$_2$] (**2**) at 323 K and (C) − [Pd(eaoac)$_2$] (**3**) at 336 K, and (D) − isotopic pattern simulation for the molecular ion [Pd(tbaoac)$_2$]$^{+\cdot}$.

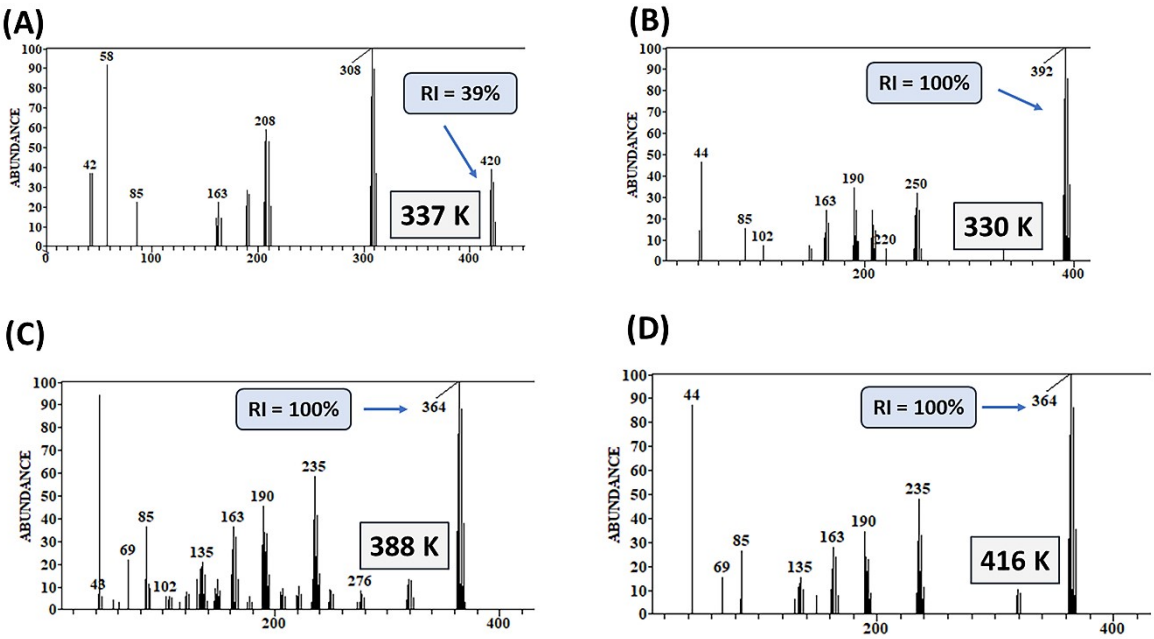

Figure S 37 EI MS spectra, where the molecular ions achieved the highest relative intensity: (A) − [Pd(tbaoac)$_2$] (**1**) at the temperature 337 K, (B) − [Pd(ipaoac)$_2$] (**2**) at 330 K and (C) − [Pd(eaoac)$_2$] (**3**) at 388 K, and (D) − at 416 K.

Table S 5 EI MS results for the complex $[Pd(tbaoac)_2]$ (**1**).

Fragments	m/z	Relative Intensity (RI) [%]			
		336 K	*342 K*	*349 K*	*365 K*
$[CHCO]^+$	41	–	2	1	1
$[CH_2{=}CO]^{+\cdot}$	42	27	48	4	4
$[CH_3CO]^+$	43	–	6	14	11
$[CH_3CHO]^{+\cdot}/[CO_2]^{+\cdot}$	44	37	51	100	100
$[CO_2H]^+$	45	–	2	11	7
$[HCOOH]^{+\cdot}$	46	–	3	64	37
$[CH_3COCH]^+/[(CH_3)_2C{=}CH_2]^{+\cdot}$	56	–	4	1	<1
$[CH_3COCH_2]^+/[^tBu]^+$	57	8	8	1	1
$[(CH_3)_2CO]^{+\cdot}/[C_4H_{10}]^{+\cdot}$	58	79	100	1	1
$[CH_3CO_2H]^{+\cdot}$	60	7	9	38	20
$[CH_3COCH_2C]^+/[^tBuC]^+$	69	–	2	–	–
$[CH_3COCH_2CO]^+/[^tBuCO]^+$	85	33	23	–	–
$[CH_3COCH_2CO_2H]^{+\cdot}/[^tBuOCHO]^+$	102	–	2	–	–
$[CH_3COCH_2C(OH)_2]^{+\cdot}/[^tBuOCHOH]^{+\cdot}$	103	21	33	–	–
$[Pd(CH_3COCH_2)]^+$	163	20	6	–	–
$[Pd(CH_3COCHCO)]^+$	190	32	5	–	–
$[Pd(CH_3COCH_2CO_2H)]^+$	208	64	7	–	–
$[Pd(CH_3COCH_2CO_2{}^tBu)]^+$	264	9	1	–	–
$[Pd(CH_3COCH_2CO_2)_2]^{+\cdot}$	308	100	5	–	–
$[Pd(CH_3COCHCO_2{}^tBu)(CH_3COCH_2CO_2)]^{+\cdot}$	364	11	1	–	–
$[Pd(CH_3COCHCO_2{}^tBu)_2]^{+\cdot}$	420	30	2	–	–

Table S 6 EI MS results for the complex [Pd(ipaoac)$_2$] (**2**).

Fragments	m/z	Relative Intensity (RI) [%]			
		323 K	*328 K*	*332 K*	*349 K*
$[CHCO]^+$	41	–	–	–	–
$[CH_2{=}CO]^{+\cdot}$	42	23	18	22	30
$[CH_3CO]^+$	43	12	9	17	9
$[CH_3CHO]^{+\cdot}/[CO_2]^{+\cdot}$	44	100	100	100	100
$[CO_2H]^+$	45	2	2	–	12
$[HCOOH]^{+\cdot}$	46	3	3	–	32
$[CH_3COCH]^+$	56	3	2	–	–
$[CH_3COCH_2]^+$	57	2	2	–	–
$[(CH_3)_2CO]^{+\cdot}$	58	7	5	–	9
$[CH_3CO_2H]^{+\cdot}$	60	4	22	–	9
$[CH_3COCH_2C]^+$	69	15	12	–	45
$[CH_3COCH_2CO]^+$	85	33	82	24	19
$[^iPrCO_2]^+$	87	9	23	–	–
$[CH_3COCH_2CO_2H]^{+\cdot}$	102	23	75	–	15
$[CH_3COCH_2C(OH)_2]^{+\cdot}$	103	9	37	–	–
$[CH_3COCH_2CO_2{}^iPr]^{+\cdot}$	144	4	22	–	–
$[Pd(CH_3COCH_2)]^+$	163	4	29	–	–
$[Pd(CH_3COCHCO)]^+$	190	2	43	–	–
$[Pd(CH_3COCH_2CO_2{}^iPr)]^+$	250	4	35	–	–
$[Pd(CH_3COCHCO_2{}^iPr)(CH_3COCHCO)]^{+\cdot}$	333	–	5	–	–
$[Pd(CH_3COCHCO_2{}^iPr)_2]^{+\cdot}$	392	7	49	98	–

Table S 7 EI MS results for the complex $[Pd(eaoac)_2]$ (**3**).

Fragments	m/z	Relative Intensity (RI) [%]				
		336 K	*339 K*	*375 K*	*419 K*	*422 K*
$[CHCO]^+$	41	–	4	–	–	–
$[CH_2CO]^{+\cdot}$	42	13	24	–	3	–
$[CH_3CO]^+$	43	12	13	12	16	14
$[CH_3CHO]^{+\cdot}/[CO_2]^{+\cdot}$	44	100	100	100	100	100
$[CO_2H]^+$	45	19	64	–	4	6
$[HCOOH]^{+\cdot}$	46	12	16	6	6	5
$[CH_3COCH]^+$	56	4	8	5	4	–
$[CH_3COCH_2]^+$	57	–	–	–	4	–
$[(CH_3)_2CO]^{+\cdot}$	58	7	9	–	–	–
$[CH_3CO_2H]^{+\cdot}$	60	–	8	–	7	8
$[CH_3COCH_2C]^+$	69	27	25	27	22	18
$[CH_3COCH_2CO]^+$	85	37	34	36	32	24
$[CH_3COCH_2CO_2H]^{+\cdot}/[OCHCO_2Et]^{+\cdot}$	102	6	6	5	6	–
$[CH_3COCH_2CO_2Et]^{+\cdot}$	130	13	14	12	13	9
$[Pd(CH_3COCH_2)]^+$	163	21	19	29	20	–
$[Pd(CH_3COCHCO)]^+$	190	22	22	32	23	–
$[Pd(CH_3COCHCOOEt)]^+$	235	27	29	40	30	–
$[Pd(CH_3COCHCO_2Et)(CH_3COCHCO)]^{+\cdot}$	319	4	5	7	7	–
$[Pd(CH_3COCHCO_2Et)_2]^{+\cdot}$	364	43	58	66	57	–

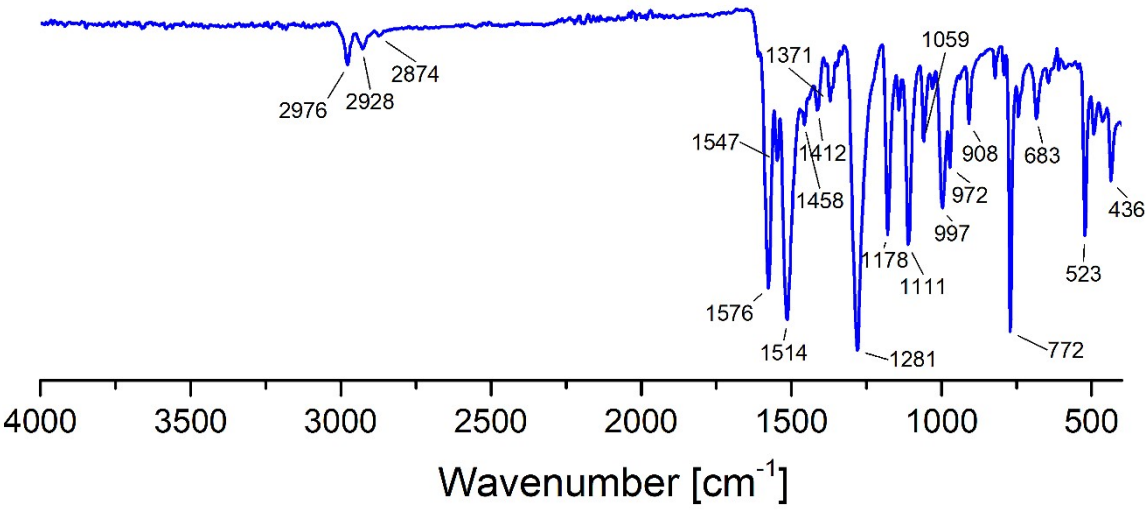

Figure S 38 Infrared spectrum for the compound [Pd(ipaoac)$_2$] (**2**) after sublimation (blue) at 353 K (p = 10^{-2} mbar).

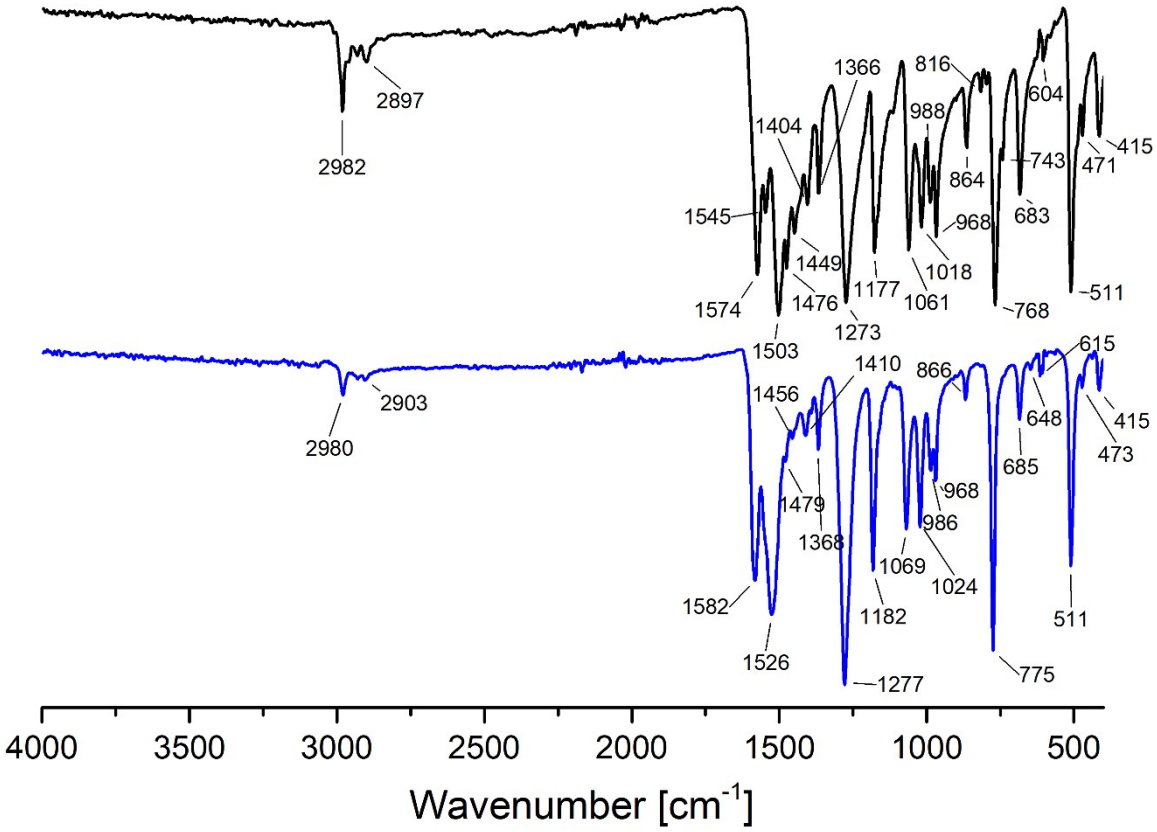

Figure S 39 Infrared spectra for the compound [Pd(eaoac)$_2$] (**3**) before (black) and after sublimation (blue) at 353 K (p = 10^{-2} mbar).

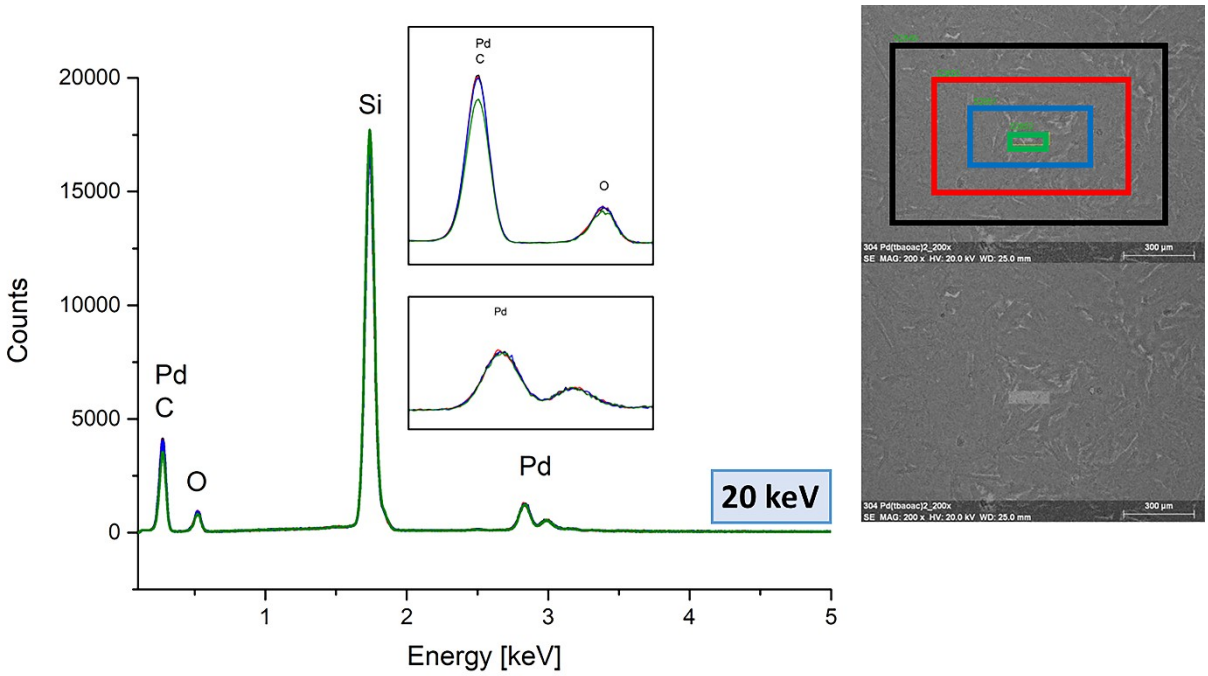

Figure S 40 Examined scan areas' EDX spectra (20 keV) for the [Pd(tbaoac)$_2$] (**1**) layer deposited on a Si(111) substrate (Mag = 200x).

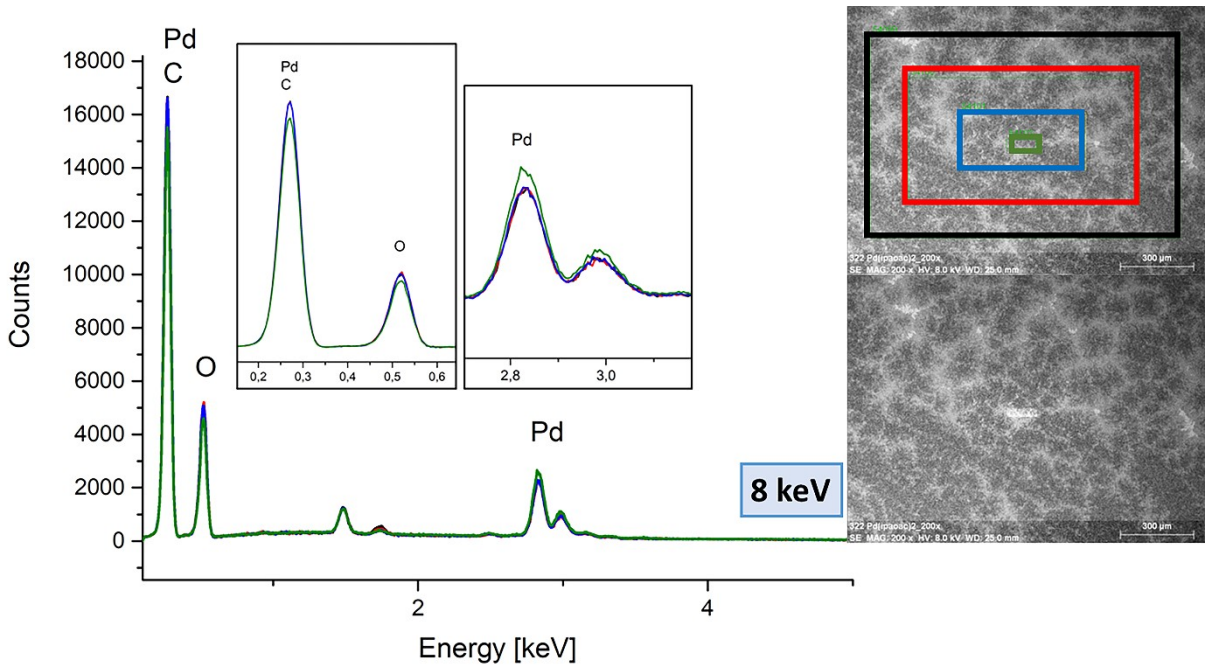

Figure S 41 Examined scan areas' EDX spectra (8 keV) for the [Pd(ipaoac)$_2$] **(2)** layer deposited on a Si(111) substrate (Mag = 200x).

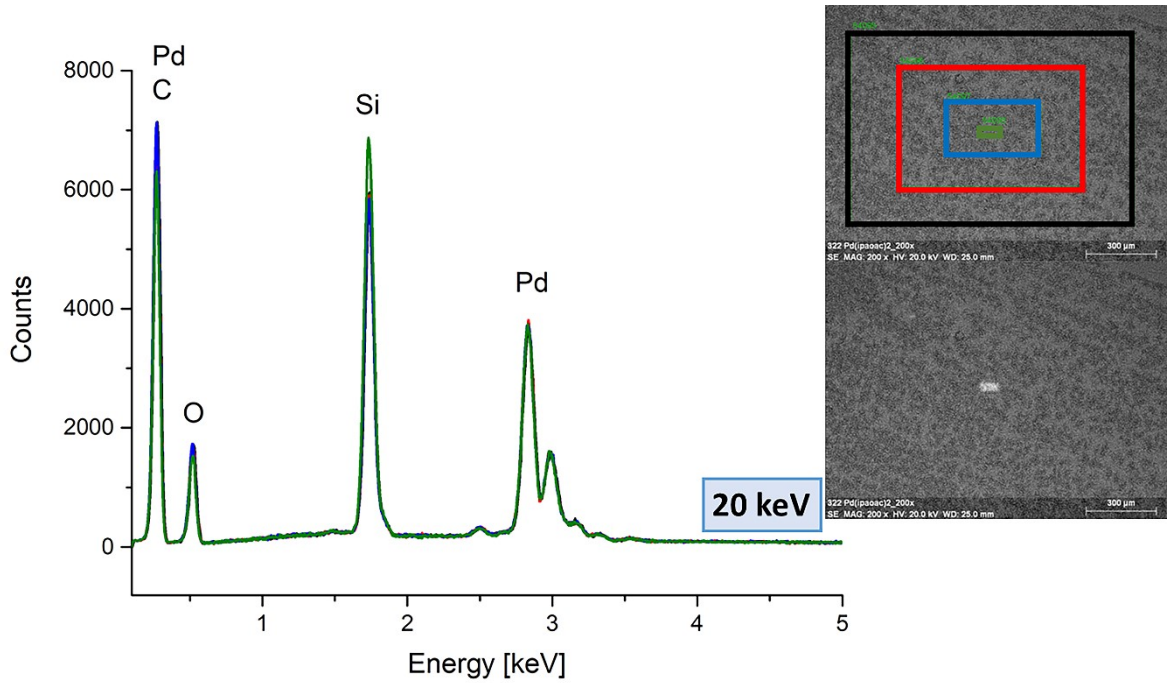

Figure S 42 Examined scan areas' EDX spectra (20 keV) for the [Pd(ipaoac)$_2$] **(2)** layer deposited on a Si(111) substrate (Mag = 200x).

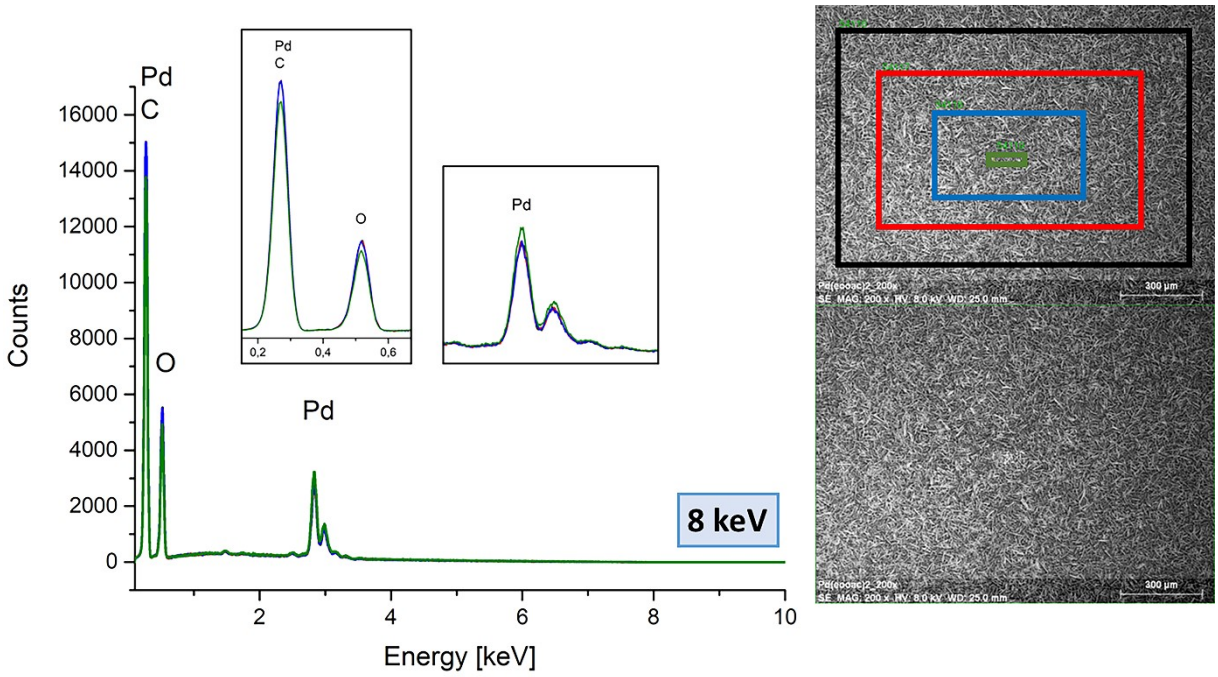

Figure S 43 Examined scan areas' EDX spectra (8 keV) for the [Pd(eaoac)$_2$] **(3)** layer deposited on a Si(111) substrate (Mag = 200x).

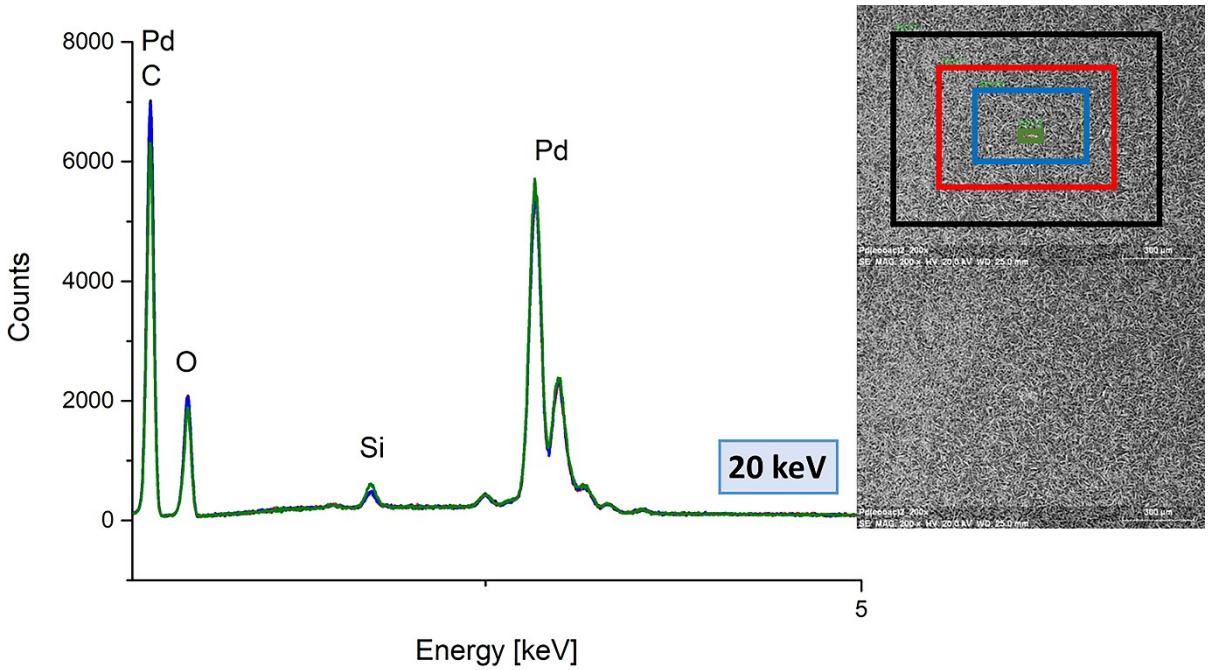

Figure S 44 Examined scan areas' EDX spectra (20 keV) for the [Pd(eaoac)$_2$] **(3)** layer deposited on a Si(111) substrate (Mag = 200x).